iScience

Article

KOLF2.1J iTF-Microglia: A standardized platform to study microglial transcriptional regulatory networks in CNS disease

Graphical abstract

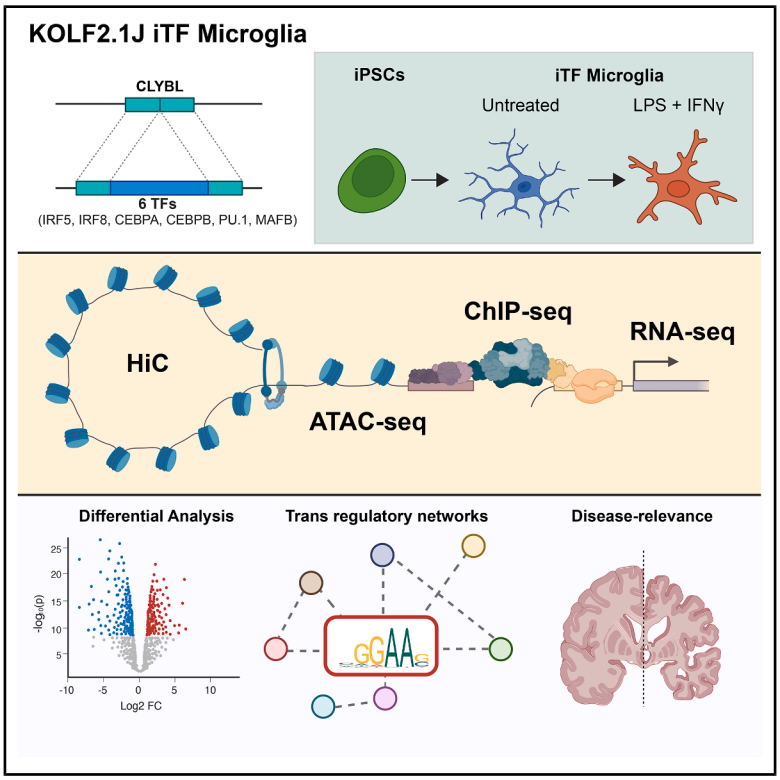

Highlights

- KOLF2.1J iTF-microglia: a stable, reproducible model of microglial gene regulation
- LPS + IFNγ triggers NF-κB, IRF< and STAT-driven inflammatory gene programs
- Mutli-omic and 3D mapping show TF and enhancer control of microglial states
- TRN and genetic analyses link microglial networks to neurodegeneration risk

Authors

Brianne B. Rogers, Ashlyn G. Anderson, Ivan Rodriguez-Nunez, ..., Kimberly M. Newberry, Richard M. Myers, J. Nicholas Cochran

Correspondence

rmyers@hudsonalpha.org (R.M.M.), ncochran@hudsonalpha.org (J.N.C.)

In brief

Neuroscience; techniques in neuroscience; stem cells research

Rogers et al., 2026, iScience *29*, 116412
July 17, 2026
https://doi.org/10.1016/j.isci.2026.116412

CellPress

iScience

CellPress
OPEN ACCESS

Article

KOLF2.1J iTF-Microglia: A standardized platform to study microglial transcriptional regulatory networks in CNS disease

Brianne B. Rogers,[1,3] Ashlyn G. Anderson,[1,2,3] Ivan Rodriguez-Nunez,[1,3] Samuel C. Bartley,[1,2] S. Quinn Johnston,[1] Jared W. Taylor,[1] Sarah K. Meadows,[1] Kimberly M. Newberry,[1] Richard M. Myers,[1,*] and J. Nicholas Cochran[1,4,*]

[1]HudsonAlpha Institute for Biotechnology, Huntsville, AL 35806, USA
[2]University of Alabama at Birmingham, Birmingham, AL 35294, USA
[3]These authors contributed equally
[4]Lead contact
*Correspondence: rmyers@hudsonalpha.org (R.M.M.), ncochran@hudsonalpha.org (J.N.C.)
https://doi.org/10.1016/j.isci.2026.116412

SUMMARY

Understanding transcriptional regulatory networks (TRNs) in microglia is essential for elucidating mechanisms underlying central nervous system (CNS) disorders. Human induced pluripotent stem cell (iPSC)-derived models enable mechanistic studies of microglia but often suffer from variability across lines. Here, we use the standardized KOLF2.1J iPSC line, engineered to inducibly express six transcription factors that allow rapid generation of microglia-like cells (iTF-microglia). We profile TRNs under homeostatic and inflammatory conditions and show that iTF-microglia resemble primary brain microglia at transcriptomic and epigenomic levels. Integrative analyses identify microglia-enriched candidate *cis*-regulatory elements (cCREs) and reveal dynamic enhancer remodeling during differentiation and stimulation with lipopolysaccharide (LPS) or interferon-gamma (IFNγ), involving NF-κB, IRF, and STAT transcription factors. TRNs active in iTF-microglia are enriched for genetic variants linked to Alzheimer's disease and related CNS disorders. These findings establish KOLF2.1J iTF-microglia as a reproducible, genetically tractable system for dissecting microglial gene regulation and TRN remodeling in disease.

INTRODUCTION

Microglia are the primary resident immune cells of the central nervous system (CNS), with essential roles in development, homeostasis, immune surveillance, and inflammation. Dysregulated microglial function is implicated in the onset and progression of various brain disorders,[1,2] and genetic risk variants associated with neurodegenerative diseases are often enriched in microglial transcriptional networks.[3] However, single-cell/nuclei RNA sequencing (RNA-seq) and ATAC sequencing (ATAC-seq) studies have underscored the transcriptional and epigenetic heterogeneity and plasticity of microglia, complicating efforts to interpret the impact of disease-risk variants.[4–13]

Microglia are challenging to study due to limited accessibility, dependence of environmental cues for maintaining tissue-specific identity, low abundance relative to other cell types, and significant interspecies differences.[14–16] Human induced pluripotent stem cells (iPSCs) have enabled the generation of microglia-like cells (shortened to "microglia" in subsequent text) through protocols that recapitulate primitive hematopoiesis with maturation in monoculture or co-culture systems.[17–23] A recent approach uses a doxycycline-inducible system to drive differentiation via six transcription factors (TFs): IRF5, IRF8, CEBPA, CEBPB, PU.1, and MAFB, with resultant cells denoted as iTF-microglia.[24] This rapid protocol produces functional microglia capable of synaptosome phagocytosis, inflammatory responses, and integration into co-culture systems with iPSC-derived neurons.[24]

iPSC-derived microglia offer several key advantages, including scalability, genetic tractability, and relevance to human biology; however, reproducibility has previously been influenced by donor-to-donor genetic variation.[25] To mitigate this limitation, the iPSC Neurodegenerative Disease Initiative (iNDI) generated the KOLF2.1J iPSC line, a genomically stable reference line designed to be neutral with respect to polygenic Alzheimer's disease (AD) risk.[26] Extensive characterization of KOLF2.1J identified heterozygous copy number variants associated with neurodevelopmental traits;[27] yet, multiple independent studies have demonstrated that this line is suitable for neurological disease modeling.[28–32] In addition, the availability of KOLF2.1J isogenic lines carrying Alzheimer's disease and related dementias variants[33] provides a robust platform for systematic genotype-to-phenotype analyses.[34]

Here, we used the KOLF2.1J iPSC line carrying an inducible six TF cassette (KOLF2.1J iTF-iPSCs), as described by Dräger et al.[24] Using this model, we investigated transcriptional regulatory networks (TRNs) governing microglial differentiation and responses to lipopolysaccharide (LPS) and interferon-γ (IFNγ). We

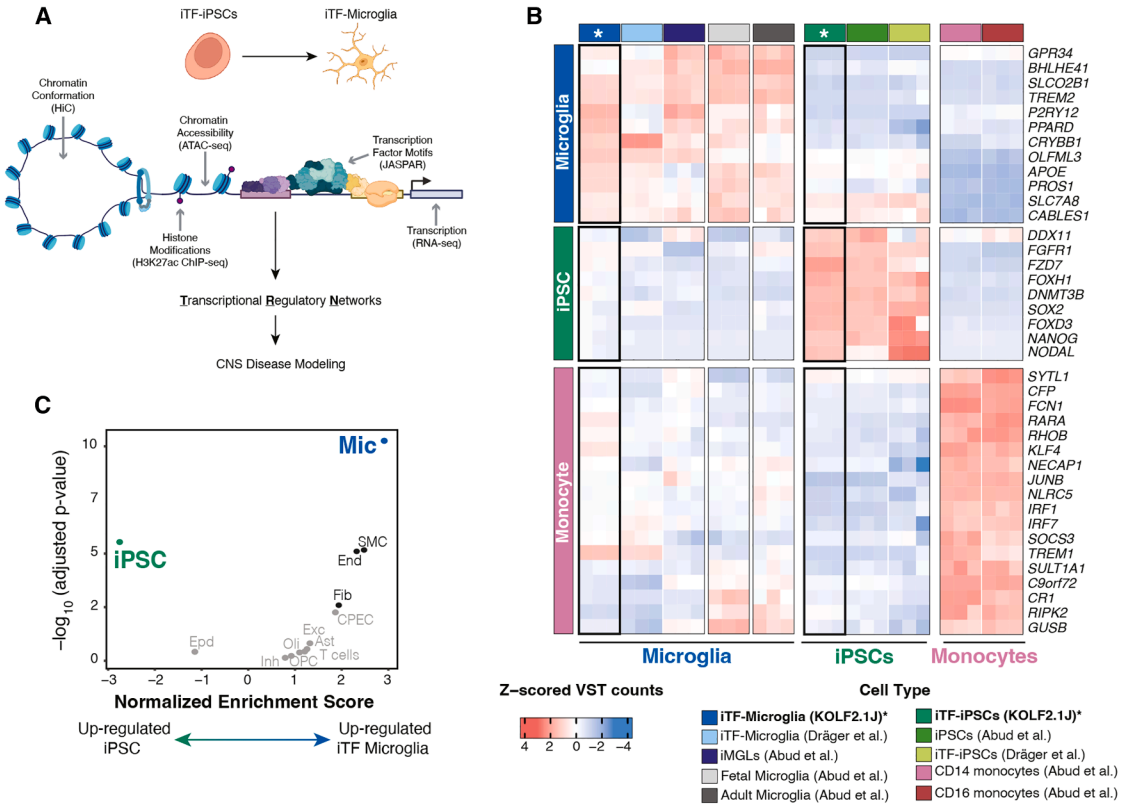

Figure 1. KOLF2.1J iTF-Microglia transcriptionally resemble primary microglia and other *in vitro* microglia models

(A) Graphical abstract of experiments performed.

(B) Heatmap of RNA-seq measured expression of cell type marker genes for Monocytes, iPSCs, and Microglia for KOLF2.1J iTF cells alongside other iPSCs,[17,24] iHPCs,[17] in vitro-derived microglia,[17,24] primary adult and fetal microglia,[17] and blood monocytes.17 Gene expression is shown as *Z* scored normalized across rows VST counts from DESeq2 to compare across previously published datasets. Columns with asterisks (*) represent cell line data generated in this study (iTF-Microglia (KOLF2.1J) and iTF-iPSCs (KOLF2.1J)).

(C) Volcano plot of GSEA performed on DESeq2-ranked genes using brain cell-type marker lists Green et al., 2024[46] and curated iPSC marker genes. Cell types include astrocytes (Asts), CNS-associated macrophages (CAMs), choroid plexus epithelial cells (CPECs), endothelial cells (Ends), ependymal cells (Epds), excitatory neurons (Excs), fibroblasts (Fibs), inhibitory neurons (Inhs), microglia (Mic), oligodendrocytes (Olis), oligodendrocyte precursor cells (OPCs), pericytes (Pers), smooth muscle cells (SMCs), T cells, and iPSCs. The normalized enrichment score (NES) reflects the degree and direction of over-representation of each marker gene set within the ranked gene list. Because NES is normalized for gene-set size, values are comparable across cell types. The plot shows NES versus $-\log_{10}$(adj. *p* value).

identified candidate *cis*-regulatory elements (cCREs), upstream TFs, and target genes, and assessed the enrichment of neurodegenerative disease risk variants within these networks, providing mechanistic insight into microglial contributions to CNS disease.

RESULTS

KOLF2.1J iTF-microglia transcriptome resembles other *in vitro* microglia models and brain microglia

Dräger et al.[24] recently reported a rapid microglia differentiation model in which iPSCs carry a cassette of six TFs that drive their conversion into microglia within eight days. This approach enables efficient differentiation, producing a relatively pure population of microglia-like cells in less time than previous methods,[17,21] while also yielding sufficient cell numbers for high-throughput functional studies. In this work, we used the KOLF2.1J iPSC line engineered to express the six-factor cassette (IRF5, IRF8, CEBPA, CEBPB, PU.1, and MAFB) from the CLYBL safe harbor locus to generate microglia. We then characterized their transcriptional and epigenetic profiles using RNA-seq, ATAC-seq, H3K27ac ChIP sequencing (ChIP-seq), and HiC to assess how well this system models *in vivo* microglia (Figure 1A).

Differentiation of KOLF2.1J iTF-iPSCs into iTF-microglia induced widespread transcriptional changes with 1,816 genes significantly upregulated (adj. *p* value $\leq$0.05 and Log2FC > 2) and 1,983 genes significantly downregulated (adj. *p* value $\leq$0.05 and Log2FC < -2). These transcriptional changes included significant upregulation of core homeostatic microglia markers such as *CX3CR1* (Log_2FC = 7.4, adj. *p* value = 2.43×10^{-8}), *P2RY12* (Log_2FC = 9.7, adj. *p* value = 5.49×10^{-15}), *TMEM119* (Log_2FC = 4.03, adj. *p* value = 1.1×10^{-4}), *TGFBR1* (Log_2FC = 3.05, adj. *p* value = 3.79×10^{-45}), *GPR34* (Log_2FC = 8.28, adj. *p* value = 1.37×10^{-10}), *MERTK*

($Log_2FC = 2.88$, adj. p value = 3.95×10^{-11}), *PROS1* ($Log_2FC = 2.23$, adj. p value = 9.34×10^{-8}), and *HEXB* ($Log_2FC = 3.14$, adj. p value = 2.95×10^{-145}; Figure S1A and S1B; Table S6).[35] Using RNA sequencing data, we compared the transcriptomic profiles of our iTF-microglia with those of previously established cell culture systems modeling microglia and their precursor cells. Based on the expression of marker genes for microglia, monocytes, and iPSCs, we analyzed iTF-microglia and iTF-iPSCs alongside two additional iPSC lines, $CD14^+$ and $CD16^+$ monocytes, induced hematopoietic progenitor cells (iHPCs), and primary adult and fetal microglia isolated from human brain tissue and cultured short term *ex vivo*.[17] All *in vitro* microglia models exhibited transcriptional profiles similar to those of primary adult and fetal microglia, characterized by high expression of microglial marker genes and low expression of monocyte and iPSC markers (Figure 1B). Principal component analysis (PCA) showed that iTF-microglia clustered together independent of iPSC background (WTC11 [Dräger et al.[24]] or KOLF2.1J). Induced microglia-like cells (iMGLs), generated over a longer (30 day) differentiation period using growth factors,[17] clustered most closely with primary microglia, whereas iHPCs (an intermediate stage in the Abud et al. differentiation protocol) and blood monocytes formed distinct clusters (Figure S1C). Expression of canonical cell-type marker genes supported these relationships, with iPSCs and iHPCs showing distinct marker profiles, monocytes exhibiting a separate transcriptional identity, and all microglial models sharing characteristic microglial signatures, with iMGLs most closely resembling primary microglia (Figures 1B, S1A, S1D, and S1E). Overall, although iTF-microglia exhibit a comparatively immature transcriptional signature relative to iMGLs and primary microglia, they nonetheless acquire a distinct microglial identity that is clearly separable from that of iHPCs and monocytes.

Gene set enrichment analysis (GSEA) revealed that genes upregulated in iTF-microglia relative to iTF-iPSCs were enriched for microglia marker genes derived from human brain single cell transcriptomic studies (adj. p value = 2.71×10^{-10}; Figure 1C).[36] Additional enrichment was observed for smooth muscle (adj. p value = 7.33×10^{-6}), endothelial (adj. p value = 7.33×10^{-6}), and fibroblast gene sets (adj. p value = 2.44×10^{-3}). Because these marker sets were derived from single-cell differential expression analyses, they capture relatively enriched programs rather than genes uniquely specific to a single lineage, and likely reflect shared cytoskeletal, extracellular matrix, and stress-response programs known to be activated in microglia rather than lineage identity.[37] In contrast, genes upregulated in iTF-iPSCs were depleted for brain cell types and showed a significant enrichment for curated pluripotent stem cell marker genes (adj. p value = 2.90×10^{-6}).

Inflammatory activation of iTF-microglia by LPS + IFNγ

Microglial activation states are key regulators of neuroinflammation and contribute to the progression of neurodegenerative diseases. To investigate how inflammatory stimulation alters transcriptional programs in our model, iTF-microglia were treated with LPS + IFNγ for 24 h on Day 17 of differentiation (Figure 2A) then assayed by RNA-seq, ATAC-seq, H3K27ac ChIP-seq, and HiC. The 24 h stimulation period was chosen to elicit a robust inflammatory response and to capture both immediate transcriptional changes and downstream regulatory programs characteristic of a sustained activation state, consistent with previous reports.[17,38,39]

LPS + IFNγ treatment in iTF-microglia resulted in large transcriptional changes with 312 genes significantly upregulated ($Log_2FC > 2$ and adj.p value ≤ 0.05) and 172 genes significantly downregulated ($Log_2FC < -2$ and adj. p value ≤ 0.05; Figures 2B and S2A–S2C). Consistent with these transcriptional changes, immunostaining for IBA1, CD11b, and phalloidin in both untreated and LPS + IFNγ-treated iTF-microglia provided complementary protein-level characterization of LPS + IFNγ treatment (Figure S2D). iTF-iPSCs were also treated with LPS + IFNγ as a control, as they should not elicit an immune response due to their low or absent expression of IFNγ pathway mediators and LPS receptors (Figure S2E). Importantly, treatment with LPS + IFNγ had no significant transcriptional effects on iTF-iPSCs (Figure S2F). To evaluate which transcriptional changes were specific to microglial response to LPS + IFNγ treatment, we compared treated iTF-iPSCs to treated iTF-microglia and found that 168 genes were significantly upregulated ($Log_2FC > 2$ and adj. p value ≤ 0.05) and 54 genes were significantly downregulated ($Log_2FC < -2$ and adj. p value ≤ 0.05; Figure S2G). Within these differentially expressed genes, an overall trend observed was that homeostatic genes were downregulated while immune response genes were significantly upregulated, such as *CXCL9* ($Log_2FC = 13.42$, adj. p value = 0.04) and *CXCL10* ($Log_2FC = 11.93$, adj. p value = 4.43×10^{-10}; involved in immune cell recruitment and neuroinflammation); *STAT1* ($Log_2FC = 3.07$, adj. p value = 5×10^{-30}) and *IRF1* ($Log_2FC = 5.09$, adj. p value = 2.07×10^{-16}); *HLA-DRB1* ($Log_2FC = 2.56$, adj. p value = 3.4×10^{-6}) and CD40 ($Log_2FC = 2.02$, adj. p value = 8.04×10^{-7}; antigen presentation); and *GBP2* ($Log_2FC = 6.67$, adj. p value = 5.74×10^{-3}; an immune defense protein induced by IFNγ; Figure 2B).[40–44] *IDO1* that encodes a metabolic enzyme linked to IFNγ responses and neurodegeneration[45] was also upregulated ($Log_2FC = 11.4$, adj. p value = 1.89×10^{-57}; Figures 2B and S2H; Table S6).

Pathway analysis of differentially expressed genes (DEGs; $Log_2FC > 2$, adj. p value ≤ 0.05) showed enrichment of immune-related pathways in iTF-microglia, including IFNγ signaling, interleukin signaling and complement regulation. These pathways were further enhanced upon LPS + IFNγ treatment. The top GO term for iTF-microglia was neutrophil degranulation, which includes many genes involved in general innate immune functions, such as vesicle trafficking, lysosomal activity, phagocytosis, and antimicrobial responses, representing core components of "homeostatic" myeloid cell biology rather than neutrophil-specific functions. In contrast, iPSCs showed enrichment for pluripotency-associated pathways (Figure S2G; Table S7).

To further contextualize these transcriptional changes in relation to human brain microglia, we compared iTF-microglia with and without LPS + IFNγ stimulation to previously identified microglial subpopulations defined by single-cell RNA-seq of postmortem human brain tissue.[46] LPS + IFNγ-treated iTF-microglia were most strongly enriched for interferon-responsive (adj. p value = 8.8×10^{-3}) and inflammatory microglial states (adj. p value = 0.016), whereas untreated

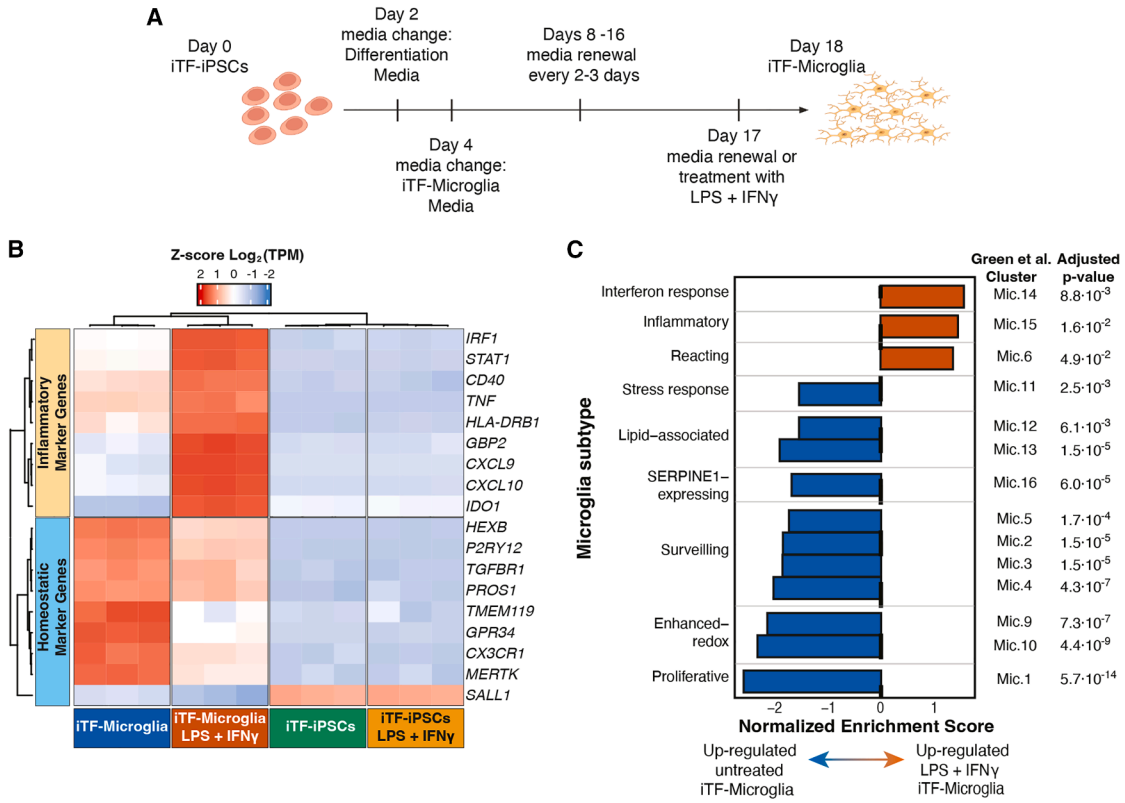

Figure 2. KOLF2.1J iTF-microglia exhibit inflammatory response under treatment with LPS + IFNγ

(A) Experimental timeline showing differentiation time from iTF-iPSCs to iTF-Microglia, including treatment time with LPS + IFNγ.

(B) Heatmap showing row *Z* scored Log_2TPM expression of key inflammatory (top) and homeostatic (bottom) marker genes for iTF-microglia (blue), LPS + IFNγ-treated iTF-microglia (orange), iTF-iPSCs (green), and LPS + IFNγ treated iTF-iPSCs (yellow).

(C) GSEA of LPS + IFNγ-treated vs. untreated iTF-microglia using gene markers for significantly enriched (adj. *p* value ≤0.05) microglial states obtained from Green et al., 2024.

iTF-microglia aligned more closely with proliferative (adj. *p* value = 5.7×10^{-14}), enhanced-redox (adj. *p* value = 4.4×10^{-9}), and surveilling subpopulations (adj. *p* value = 4.3×10^{-7} - 1.7×10^{-4}; Figure 2C). This pattern is consistent with prior single-cell studies distinguishing IFN-like and NF-κB-associated microglial activation programs and suggests that LPS + IFNγ stimulation primarily captures later, integrated inflammatory and interferon-responsive states rather than transient signaling responses.[46]

Cis-regulatory landscapes of iTF-microglia across differentiation and activation

To characterize gene regulatory changes accompanying differentiation into microglia and subsequent inflammatory stimulation, we performed ATAC-seq and H3K27ac ChIP-seq in iTF-iPSCs, iTF-microglia, and LPS + IFNγ-treated iTF-microglia (Figure S3A and S3B). Chromatin accessibility together with H3K27ac enrichment provides useful indicators for predicting active cCREs, including potential enhancers and promoters.[47] Overlapping chromatin accessibility with H3K27ac peaks, we identified 37,256 cCREs in iTF-iPSCs, 47,350 in iTF-microglia, and 46,821 in LPS + IFNγ-treated iTF-microglia (Table S4). While 13,075 cCREs were shared across cell types, most cCREs were cell type-specific (23,787 cCREs in iTF-microglia with or without LPS + IFNγ and 22,679 cCREs in iTF-iPSCs; Figure 3A). Cell type-specific cCREs were enriched for distal enhancer-like sequences (dELS; Chi-squared adj. *p* value $<2.2 \times 10^{-16}$ for both cell types) from ENCODE4 (Figure 3A).[48] In contrast, cCREs shared across iTF-iPSCs, iTF-microglia, and LPS + IFNγ-treated iTF-microglia were predominantly proximal enhancer-like sequences (pELS, 67%) and promoter-like sequences (PLS, 12%). Functional enrichment analysis revealed that cCREs in iTF-iPSCs were associated with pluripotency pathways, while cCREs shared by untreated and LPS + IFNγ--treated iTF-microglia were enriched for immune pathways (Table S8). LPS + IFNγ-specific cCREs were particularly enriched for chemokine and cytokine signaling, while cCREs common to iTF-iPSCs, untreated iTF-microglia and LPS + IFNγ-treated iTF-microglia were linked to core cellular functions, such as RNA processing, protein translation, and cell cycle regulation (Table S8).

Among the identified cCREs, we found overlapping ATAC-seq and H3K27ac peaks at both ends of the *NANOG* gene in iTF-iPSCs, a TF used as a pluripotency marker (Figure 3B).[49] In contrast, *TREM2*, a gene expressed in microglia and implicated

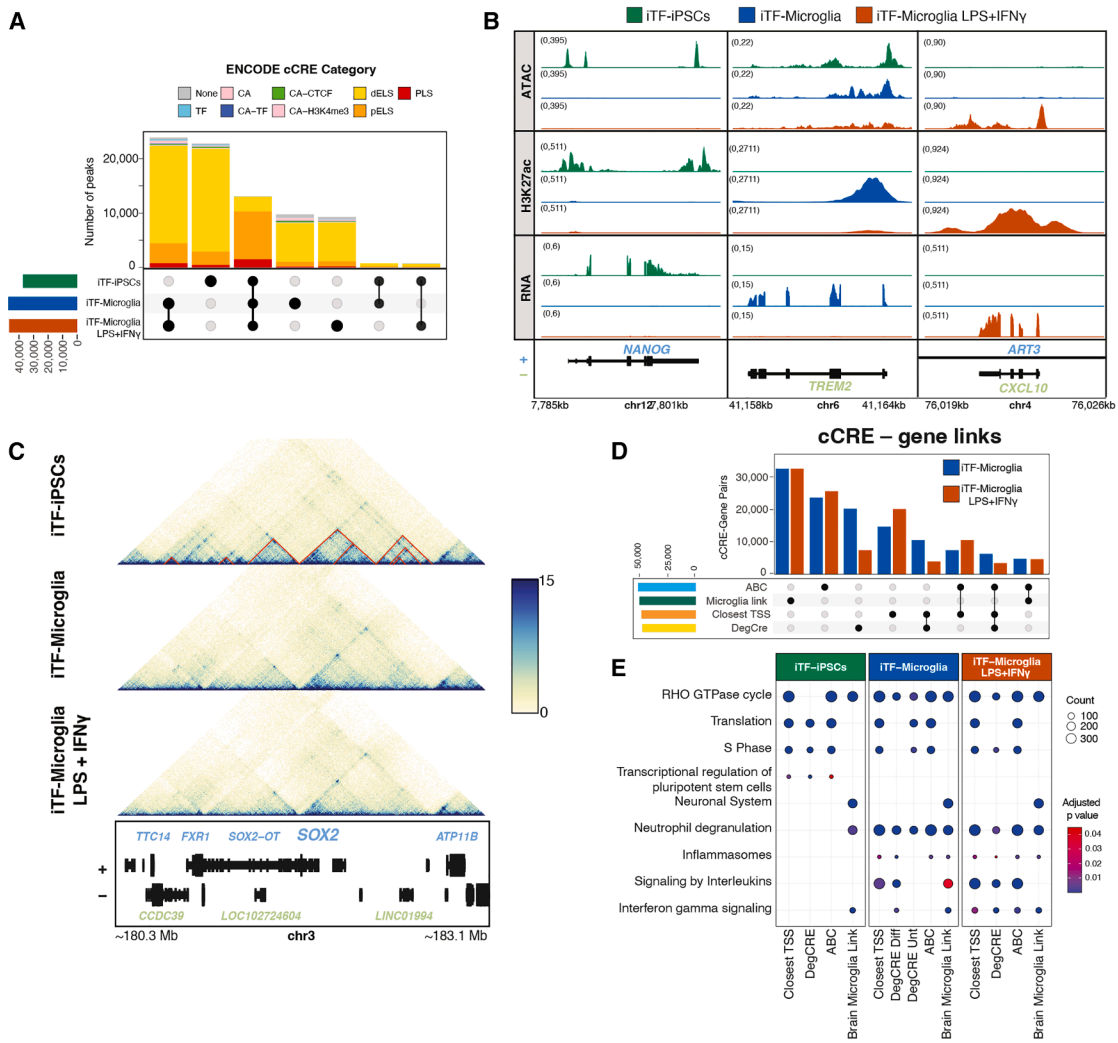

Figure 3. KOLF2.1J iTF-microglia cCREs are enriched for immune response pathways

(A) Upset plot of overlap of cCREs (presence of both ATAC-seq and H3K27ac peak) identified in iTF-iPSCs, untreated iTF-microglia, and LPS + IFNγ-treated iTF-microglia, annotated using ENCODE4 categories: CA (chromatin accessibility), CA-CTCF (CA with CTCF binding), dELS (distal enhancer-like sequence), PLS (promoter-like sequence), TF (TF binding), CA-TF (CA with TF binding), CA-H3K4me3 (CA with H3K4me3), and pELS (proximal enhancer-like sequence). Horizontal bars indicate the number of cCRE identified in each cell type/treatment. Vertical bars indicate the number of shared cCREs identified in multiple cell types, denoted by connected black dots below the vertical bars.

(B) Representative genome browser tracks showing ATAC-seq, H3K27ac, and RNA-seq signal at *NANOG*, *TREM2*, and *CXCL10* loci.

(C) Five kilobase resolution HiC interaction matrix of the *SOX2* locus in the iTF-iPSC, iTF-microglia, and LPS + IFNγ-treated iTF-microglia cell states. Red lines indicate significant domain calls in each HiC dataset. Red lines indicate topologically associated domains (TADs).

(D) UpSet plot of overlap of cCRE-to-gene associations identified by four mapping strategies in untreated and LPS + IFNγ-treated iTF-microglia. The horizontal bars represent the total number of cCRE-to-gene associations identified by each mapping strategy. The vertical bars indicate the number of cCRE-to-gene associations (colored by cCRE type) identified by multiple mapping strategies, denoted by connected dots below the vertical bars.

(E) Reactome pathway enrichment of predicted target genes across cell states and mapping methods. Pathways were identified using compareCluster (p value <0.05) and plotted pathways were manually selected from the significantly enriched terms.

in AD and Nasu-Hakola disease pathogenesis,[50] showed similar chromatin accessibility across iTF-iPSCs, untreated iTF-microglia, and LPS + IFNγ-treated iTF-microglia, while an H3K27ac peak was only present in untreated iTF-microglia, indicating cCRE activity specifically in iTF-microglia. Loss of this peak in LPS + IFNγ-treated iTF-microglia correlated with strong *TREM2* downregulation (Figure 3B; iTF-microglia avg. TPM = 329 vs. LPS + IFNγ-treated iTF-microglia avg. TPM = 2.93). In contrast, the early-response IFNγ gene *CXCL10*[40] showed an active cCRE signature exclusively in LPS + IFNγ-treated iTF-microglia (Figure 3B).

Inference of cCRE-gene associations across microglial states

Assigning distal CREs to their target genes is a critical yet complex task for understanding gene regulation. While the most

common approach assigns enhancers to the closest gene, many enhancers often bypass the nearest gene to regulate more distal ones, limiting the accuracy of proximity-based approaches alone.[51] To directly interrogate chromatin looping relationships underlying cCRE-gene interactions across microglial differentiation and inflammatory activation, we generated genome-wide Hi-C chromatin conformation maps in KOLF2.1J iTF-iPSCs, iTF-microglia, and LPS + IFNγ-treated iTF-microglia. These data capture three-dimensional chromatin organization in each cell type and state and enable linkage of distal regulatory elements to putative target promoters based on physical proximity in 3D genome space (Figure 3C).

To leverage these data and to integrate complementary approaches, we applied four distinct strategies that rely on distinct biological and computational assumptions: (1) closest gene, (2) DegCre, (3) activity-by-contact (ABC), and (4) brain microglia links. The closest gene approach provides a simple distance-based baseline without regulatory inference. DegCre leverages coordinated changes in gene expression and chromatin accessibility to probabilistically link differentially accessible cCREs to differentially expressed genes. The ABC model integrates enhancer activity with three-dimensional chromatin contact frequency derived from Hi-C data generated in this study to predict enhancer-gene pairs. Brain microglia links, derived from single-nucleus RNA-seq and ATAC-seq of postmortem human dorsolateral prefrontal cortex tissue, capture microglia regulatory relationships based on correlated variation in chromatin accessibility and gene expression *in vivo*. Collectively, these complementary strategies integrate three-dimensional genome architecture, regulatory activity, and *in vivo* microglial context to identify a robust set of candidate cCRE-gene associations.

Notably, cCREs identified in both untreated and LPS + IFNγ-treated iTF-microglia showed significantly greater overlap with brain microglia cCREs derived from postmortem human tissue[5] compared to cCREs identified in iTF-iPSCs (Fisher's exact test, untreated, odds ratio = 1.95, $p < 2.2 \times 10^{-16}$; treated, odds ratio = 2.88, $p < 2.2 \times 10^{-16}$). For DegCre, we used differential chromatin accessibility to map cCRE-to-gene associations involved in microglial differentiation (iTF-iPSCs vs. iTF-microglia), and H3K27ac changes to infer inflammatory CRE-gene associations (LPS + IFNγ-treated iTF-microglia vs. untreated iTF-microglia; Figures S3C–S3F). The distribution of the distances between cCREs and their predicted target genes peaked at TSS and distal regions around 100 kb from TSS (Figure S4A).

Most cCRE-gene associations were method-specific, with limited overlap across approaches (Figures 3D and S4B). The ABC model and brain microglia links preferentially assigned promoter-associated cCREs (−2 kb to +0.2 kb from GENCODE v46 TSS), consistent with the higher ATAC-seq and H3K27ac signal observed at promoters relative to enhancers (Figure S4C). In contrast, DegCre more frequently linked distal enhancer-associated cCREs by coupling differential gene expression with changes in chromatin accessibility and H3K27ac, which predominantly occur at distal enhancers (Figure S4B). Together, these approaches capture distinct classes of cCRE-gene relationships and, in aggregate, provide a more comprehensive view of TRNs in microglia.

Using cCRE-gene links derived from the four complementary approaches, pathway enrichment analysis (Figure 3E; Table S9) revealed that cCRE-associated genes in iTF-iPSCs, iTF-microglia, and LPS + IFNγ-treated iTF-microglia were enriched for protein translation and S-phase proliferation pathways, which were largely absent in brain microglia. In contrast, brain microglia cCRE-gene associations were enriched for neuronal system pathways, likely reflecting differences between *in vitro* culture conditions and postmortem brain tissue environments. Despite these differences, several regulatory programs were shared across conditions. The RHO GTPase cycle, which regulates cytoskeletal organization and intracellular signaling, was consistently enriched, highlighting conserved regulatory functions across microglial states. Immune-related pathways showed state-dependent patterns: neutrophil degranulation, inflammasome signaling, and interleukin signaling were enriched in both iTF-microglia and brain microglia, whereas IFNγ signaling was most strongly enriched in LPS + IFNγ-treated iTF-microglia and brain microglia, consistent with activation-associated regulatory programs. Together, these complementary cCRE-gene linking approaches demonstrate that integrating regulatory activity, chromatin architecture, and *in vivo* microglial context provides a more nuanced and biologically grounded view of gene regulatory programs underlying microglial identity and activation.

TFs shape microglial identity and response in iTF-microglia

TF binding at CREs plays a central role in regulating gene expression. Lineage-determining TFs are essential for initiating and maintaining open chromatin states associated with cell identity, while signal-dependent TFs adapt gene expression in response to external cues.[52] The transcriptional and *cis*-regulatory changes observed during iTF-microglia differentiation and LPS + IFNγ stimulation therefore imply coordinated alterations in the programs that drive microglial activation. In macrophages, inflammatory responses are marked by changes in H3K27ac levels at enhancers, which are enriched for binding motifs of TFs involved in immune signaling.[53] Notably, H3K27ac has also been implicated in microglial immune memory following LPS exposure.[54]

Here, TRNs are defined as inferred, condition-specific relationships linking TFs to active CREs and their predicted target genes, based on integrated analyses of motif enrichment, chromatin accessibility, H3K27ac, gene expression, and cCRE-gene associations (Figure 4A). To identify candidate TFs driving microglial identity and inflammatory responses, we applied randomized lasso stability selection approach using the monaLisa package.[55] This uncovered TF motifs associated with chromatin accessibility changes during differentiation (iTF-iPSCs vs. iTF-microglia) and H3K27ac remodeling upon stimulation (LPS + IFNγ-treated iTF-microglia vs. iTF-microglia; Figure 4B).

cCREs more accessible in iTF-iPSCs were enriched for motifs of SOX and POU TF families, key regulators of pluripotency, self-renewal, and reprogramming,[56,57] as well as TEAD motifs, known to enhance iPSC reprogramming efficiency.[58] In contrast, cCREs active in iTF-microglia were enriched for ETS and C/EBP motifs, including PU.1 (*SPI1*) and CEBPA,

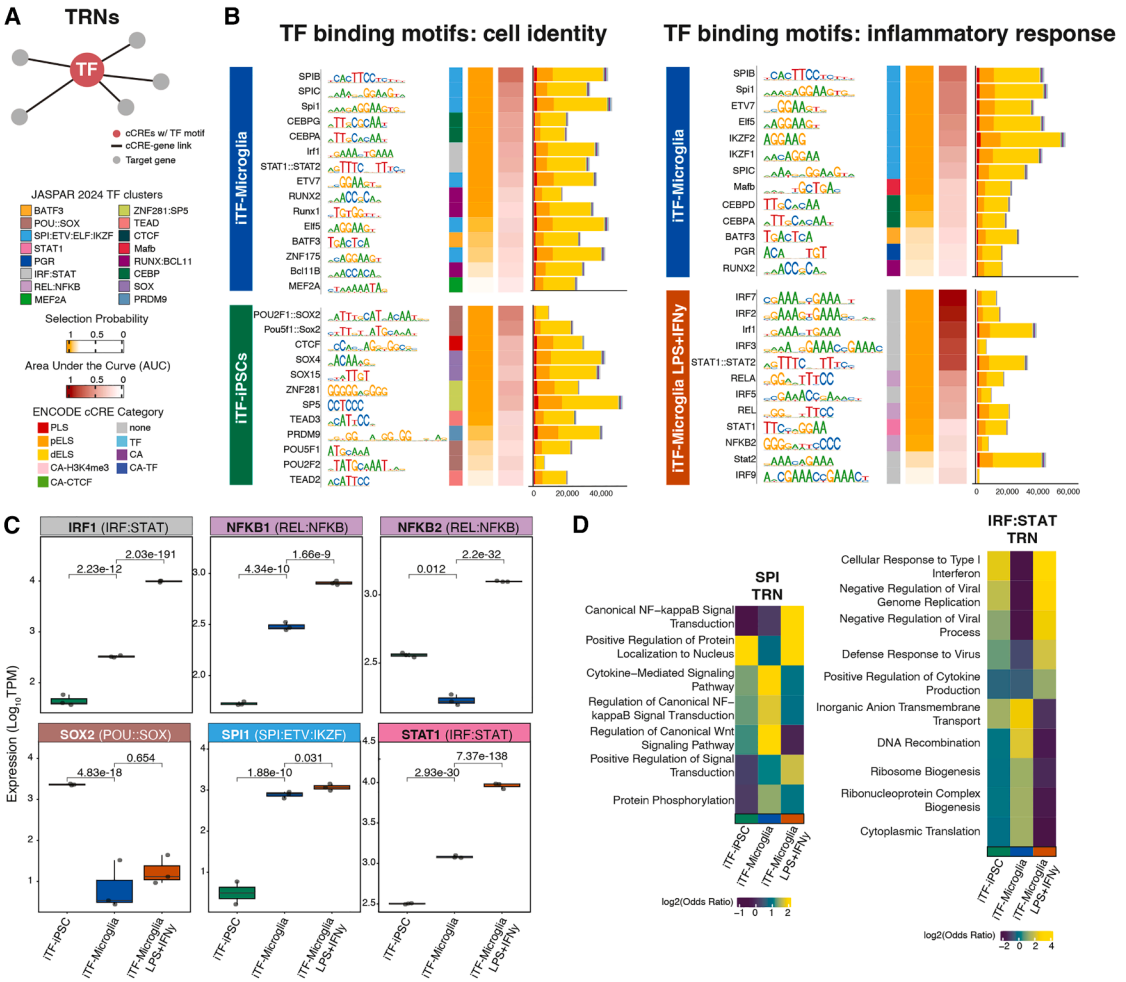

Figure 4. TF motifs linked to microglial differentiation and inflammatory response

(A) Diagram depicting TRNs strategy within our dataset.

(B) TF motifs enriched in cCREs with different chromatin accessibility between iTF-iPSCs and iTF-microglia (left). Motifs are ranked by selection probability and area under the curve (AUC) from randomized lasso stability selection; corresponding ENCODE annotations are shown. TF motifs enriched in cCREs with different H3K27ac signal between LPS + IFNγ-treated and untreated iTF-microglia (right).

(C) Expression (Log_{10} TPM) of representative TFs from highly represented JASPAR2024 motif clusters. DESeq2 *p* values shown between comparisons. Each point represents an individual replicate. Boxes indicate the interquartile range (IQR), center lines indicate the median, and whiskers extend to 1.5*x* the IQR.

(D) Heatmaps showing GO biological process enrichment for genes concordantly linked (ABC + DegCre) to cCREs containing SPI-family (left) or IRF/STAT (right) motifs in iTF-iPSCs, untreated iTF-microglia, and LPS + IFNγ-treated iTF-microglia. Enrichment was calculated using a hypergeometric test with a background of all genes concordantly linked within the corresponding cell type/state.

lineage-determining TFs essential for microglia development[59] and both encoded by the iTF cassette inserted into KOLF2.1J cells (Figure 4B). These motif enrichments are consistent with prior epigenomic profiling of primary human microglia.[14] Comparison of LPS + IFNγ-treated versus untreated iTF-microglia revealed that cCREs with higher H3K27ac in the untreated state were enriched for motifs of homeostatic TFs such as RUNX2, MAFB, and IKZF1, which are implicated in maintaining microglial identity and modulating neurodegeneration.[9,14,60,61] PU.1 (*SPI1*) and CEBPA motifs were also found, consistent with their dual roles in homeostasis and inflammation.[62–64] In contrast, cCREs with increased H3K27ac upon LPS + IFNγ treatment were enriched for NF-κB, IRFs, and STATs motifs, signal-dependent TFs that mediate microglial inflammatory responses (Figure 4B).[65–67]

Because lasso regression may select only a subset of correlated motifs within motif clusters, we additionally examined the expression of TFs corresponding to the seven most represented JASPAR2024 motif clusters. These clusters group families of similar binding motifs and were identified by monaLisa, allowing us to prioritize the most likely drivers of these TRNs (Figure S5A). For example, ELF5 motifs (SPI/ETV/ELF cluster) were enriched in untreated iTF-microglia, yet *ELF5* itself showed low expression in both iTF-iPSCs and iTF-microglia (both TPM <0.1). In contrast, SPI1, which clusters within the same motif family, was significantly up-regulated in microglia compared to iTF-iPSC (adj. *p*

value = 1.88×10^{-10}) and is a known regulator of microglial gene expression, indicating that SPI1 is the likely coordinator of this TRN in iTF-microglia (Figure 4C). Similarly, IRF1 and STAT1, central members of the IRF/STAT cluster, were strongly up-regulated in LPS + IFNγ-treated microglia compared to untreated cells (IRF1, adj. p value = 2.03×10^{-191}; STAT1, adj. p value = 7.37×10^{-138}), consistent with activation of inflammatory transcriptional programs in stimulated microglia (Figure 4C).

To define the functional roles of these TRNs, we analyzed concordant ABC + DegCre-linked genes from cCREs containing SPI-family or IRF/STAT motifs (Figure 4B). The SPI-family TRN, enriched in untreated microglia, were linked to genes involved in cytokine-mediated signaling, regulation of NF-κB signaling, and Wnt signaling, while in treated microglia they were enriched for NF-κB signal transduction and regulation of protein localization to the nucleus (Figure 4D). In contrast, the IRF/STAT TRN, preferentially enriched in LPS + IFNγ-treated microglia, were linked to genes involved in type I interferon response, viral defense, and cytokine production, whereas in untreated microglia they showed enrichment primarily for translation and ribosome biogenesis (Figure 4D). Together, this indicates that SPI-family TRNs contribute to baseline microglial signaling programs with context-dependent shifts upon stimulation, while IRF/STAT TRNs preferentially regulate activation-associated interferon responses.

iTF-microglia TRNs are enriched for neurodegenerative and autoimmune risk variants

GWAS have identified many genomic loci associated with disease risk; yet, linking these to specific variants, genes, molecular pathways, and relevant cell types remains challenging. Notably, active CREs in brain microglia have been shown to be significantly enriched for neurodegenerative disease heritability.[5,68] To assess disease associations within iTF-iPSCs and iTF-microglia (with or without LPS + IFNγ) TRNs, we evaluated heritability enrichments using GWAS summary statistics of various diseases and stratified linkage disequilibrium (LD) score regression (sLDSC).[69,70]

sLDSC analysis demonstrated that cCREs, defined by overlapping ATAC-seq and H3K27ac peaks, showed stronger heritability enrichment than either modality alone (Figure 5A). Among these cCREs, those from both untreated and LPS + IFNγ-treated iTF-microglia were enriched for AD and MS heritability, whereas iTF-iPSC cCREs were enriched for bipolar disorder (BD) and schizophrenia (SCZ) variants (Figure 5A; Table S10). To determine whether disease heritability further concentrates within specific regulatory programs, we grouped cCREs by TRNs. SPI/ETV and IRF/STAT TRNs were enriched for both AD and MS heritability (Figure 5B). Importantly, SPI/ETV-associated networks broadly marked microglial regulatory programs, whereas IRF/STAT networks were more strongly represented in stimulated microglia (Figure 4D). In contrast, POU/SOX TRNs were predominantly enriched for MS heritability (Figure 5B). Notably, MAFB, a key regulator of adult microglial gene expression with prior associations to AD,[5] is part of the POU/SOX network and also demonstrated enrichment for AD heritability. REL/NFKB TRNs were enriched for MS and for immune-related diseases including inflammatory bowel disease (IBD) and systemic lupus erythematosus (SLE, Figure 5B). In addition, transcriptome-based enrichment analyses using MAGMA[71] mirrored the TRN-level disease associations. Genes up-regulated in untreated iTF-microglia were enriched for AD risk variants from multiple GWAS datasets, whereas genes up-regulated in LPS + IFNγ-treated iTF-microglia were enriched for variants from one AD GWAS (Jensen et al.) as well as for MS, IBD, and SLE (Figure S5B). While enrichment analyses were performed independently for each trait, prior studies have shown that a limited number of risk loci are shared across neurodegenerative diseases, consistent with partially overlapping but largely disease-specific genetic architectures. These results indicate that AD and MS heritability localizes to distinct microglial transcriptional programs spanning both homeostatic and activation-associated states.

Having identified disease-enriched regulatory programs, we next asked whether individual AD-associated variants within iTF-microglia cCREs are predicted to disrupt TF binding. We used motifbreakR[72] to predict the effects of AD GWAS variants on TF binding motifs (Table S12). Within our microglia cCREs, 162 AD GWAS variants had a predicted effect on binding, with the most effects observed in CTCF, SP4, and ZNF281 motifs (Figure S5C). To assess whether these AD GWAS variants within iTF-microglia cCREs exhibit altered TF binding in human brain, we additionally examined allele-specific binding (ASB) events for 94 TFs profiled across nine brain regions.[73] Although these data are derived from bulk brain tissue and therefore reflect signals across multiple cell types rather than microglia alone, and assess a more limited set of TFs compared to the broader motif set analyzed by motifbreakR, the strongest ASB signals were observed for CTCF and RAD21, a cohesin complex component that frequently colocalizes with CTCF. (Figure S5D). These observations are consistent with our motif predictions and support potential disruption of chromatin regulatory architecture at AD-associated loci.

To illustrate how these regulatory enrichments resolve at specific loci, we examined representative AD-associated variants that have been functionally validated in prior studies with convergent motif, cCRE, and cCRE-gene linkage evidence (Table S11). rs9357347, a functionally characterized AD-associated variant previously linked to to altered *TREM2* and *TREML1* expression and reduced AD risk,[74,75] was located in a cCRE identified in both untreated and LPS + IFNγ-treated iTF-microglia. It was linked to *TREM2* and *TREML2* in untreated iTF-microglia via DegCre (Figure 5D). Notably, *TREM2* expression and H3K27ac signal at this locus were higher in untreated iTF-microglia compared to stimulated cells. Motif analysis predicted that rs9357347 creates a ZNF343 binding motif within this cCRE, consistent with prior functional data showing its association with increased *TREM2* expression and a reduced risk of Alzheimer's disease.

Two AD-associated variants, rs6733839 and rs72838287, reside within the same microglia-specific cCRE at the *BIN1* locus (Figure 5E). This cCRE was present in both untreated and LPS + IFNγ-treated iTF-microglia and was linked to *BIN1* via both DegCre and ABC. Motif analysis revealed allele-specific TF

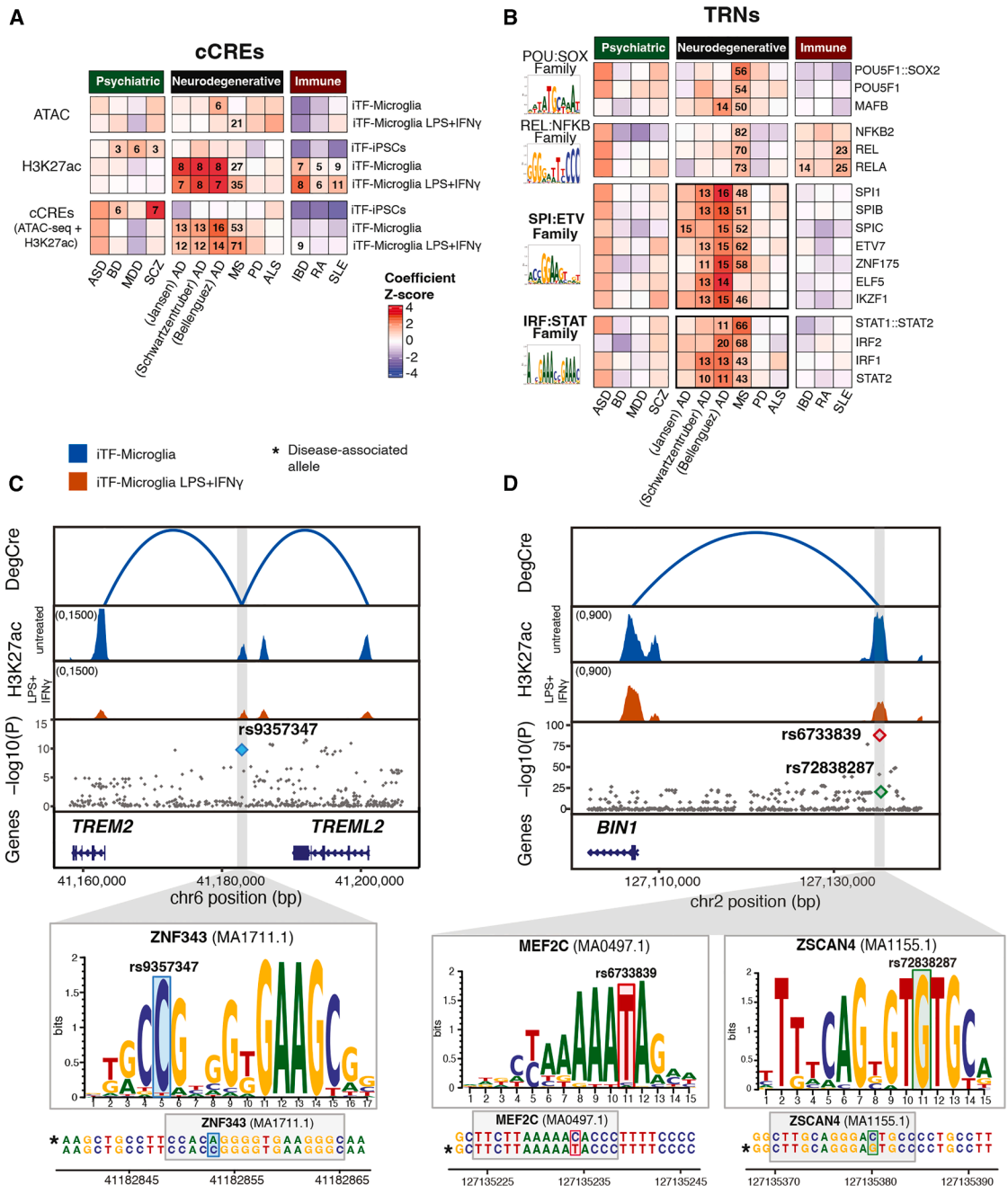

Figure 5. Mapping disease-risk variants to KOLF2.1J TRNs

(A and B) Heatmap of sLDSC coefficient *Z* scores for (A) cCREs (ATAC-seq peaks and H3K27ac peaks) and (B) TRNs across conditions. Feature-disease pairs with significant coefficients (Benjamini-Hochberg corrected $p < 0.05$) are annotated with their enrichment scores. Exact coefficients, enrichment estimates, and adjusted *p* values are provided in Table S10.

(C and D) Linkage plots showing cCREs containing risk variants and their predicted target genes (C) *TREM2* and (D) *BIN1* based on DegCre and ABC models. Signal tracks show bigwigs for H3K27ac in treated and untreated microglia. Bellenguez et al. 2022 AD GWAS –log10(*p* values) shown for each locus. Predicted motifbreakR effect for highlighted SNPs. Asterisks indicate alleles associated with an increased risk of AD.

effects at both variants. The disease-associated allele at rs6733839 was predicted to create a MEF2C motif, whereas the disease-associated allele at rs72838287 was predicted to create a ZSCAN4 motif. Prior MPRA experiments in THP1-derived macrophages demonstrated allelic differential activity for rs72838287,[76] supporting functional regulatory effects at this enhancer. Together, these examples demonstrate that iTF-microglia capture regulatory architecture at well-established

AD risk loci. The convergence of cCRE accessibility, motif-altering variants, cCRE-gene linkage, and concordant expression patterns supports the biological fidelity of the iTF-microglia model and its utility for dissecting the regulatory mechanisms underlying AD risk.

DISCUSSION

Human iPSC-derived microglia have become an increasingly important system for interrogating the genetic and molecular mechanisms underlying neurodegenerative disease risk. However, the utility of these models depends both on how faithfully they recapitulate microglial identity and on whether their regulatory landscapes enable mechanistic interpretation of disease-associated genetic variation. Here, we characterize a dox-inducible iTF microglia model in the KOLF2.1J genetic background. We generate an integrated multi-omic resource, including RNA-seq, ATAC-seq, H3K27ac ChIP-seq, and HiC, at the iPSC stage, after differentiation, and upon LPS + IFNγ stimulation. These data in aggregate define TRNs across microglial differentiation and inflammatory activation.

KOLF2.1J iTF-microglia acquire a transcriptional profile consistent with other iPSC-derived microglia models and with primary human microglia. iTF-microglia generated from KOLF2.1Js closely resemble iTF-microglia generated from other iPSC lines, indicating that differentiation strategy, rather than genetic background, is the primary determinant of transcriptional identity. While growth factor-based protocols for iPSC-derived microglia more closely resemble transcriptional profiles of primary microglia, iTF-microglia were clearly distinct from monocytes and were enriched for microglia marker genes. Importantly, the inducible TF differentiation substantially reduced differentiation time relative to growth factor-only approaches, offering a practical advantage for high-throughput functional studies.

Our combined LPS + IFNγ stimulation was chosen to elicit a robust and synergistic inflammatory response that engages both NF-κB-driven (LPS-like) and STAT/IRF-driven (interferon-like) transcriptional programs, and has been shown to promote inflammatory neurodegeneration.[65] These pathways are tightly interconnected: IFNγ can potentiate NF-κB activation by increasing accessibility at NF-κB-responsive enhancers, while NF-κB induces IRF family members that amplify interferon-responsive genes. Conversely, several interferon-stimulated genes dampen NF-κB activity, highlighting the bidirectional and temporally dynamic nature of this cross-regulation.[77,78] Modeling this regulatory interplay *in vitro* is therefore critical for understanding how microglial activation reshapes gene regulatory programs in disease-relevant contexts. Consistent with this, LPS + IFNγ treatment in iTF-microglia led to downregulation of homeostatic genes and upregulation of pathways associated with brain aging and neurodegeneration, including interferon signaling, complement regulation, and antigen presentation.[79,80] These transcriptional changes were accompanied by coordinated epigenetic remodeling, as we observed increased H3K27ac at cCREs, which in turn were enriched for NF-κB, IRF, and STAT motifs, supporting coordinated activation of these inflammatory regulators.

In this study, we generated genome-wide HiC maps across iTF-iPSCs, iTF-microglia, and inflammatory microglia to interrogate three-dimensional chromatin organization across cellular states. Incorporating these data into ABC modeling enabled us to link CREs to putative target genes. When compared with differential- and correlative-based approaches, HiC-informed associations captured both distal enhancer-gene interactions and promoter-promoter contacts, potentially reflecting higher-order TFs with clusters of Pol II activity. In contrast, differential-based approaches primarily capture distal enhancer relationships associated with state-specific activity. These distinctions underscore that no single strategy fully resolves regulatory architecture. Rather, integrating orthogonal data types provides a more comprehensive view of microglial gene regulation, capturing complementary features of enhancer-promoter connectivity and higher-order chromatin organization.

We constructed state-resolved TRNs that link upstream TF to cCREs and downstream target genes, thereby defining coordinated regulatory programs in untreated and inflammatory microglia. These networks delineate distinct microglial states, including an SPI:ETV:ELF-centered program in untreated cells and an IRF:STAT-driven program following LPS + IFNγ stimulation. Partitioned heritability analyses demonstrated that cCREs within both networks are significantly enriched for AD and MS risk variants, indicating that disease-associated genetic variation is concentrated within core microglial regulatory networks rather than isolated loci. Importantly, AD risk variants were enriched within TRNs defined in both untreated and inflammatory microglia, supporting a role for diverse microglial regulatory states in shaping AD-associated genetic signal.

We further identified specific TFs likely mediating genetic risk through disruption of binding motifs within microglial cCREs. Several SPI family members (SPI1, ETVs, ELFs) were associated with AD heritability enrichment,[81] with SPI1 being a known AD risk gene.[82] MAFB and IKZF1 were also linked to AD,[5,12] while NF-kB, IRF, and STAT TFs have been implicated in various neurodegenerative diseases.[83–85] However, validation of allele-specific TF binding in microglia remains limited, in part due to the scarcity of TF ChIP-seq data in microglia.[73,86]

Consistent with these motif-level observations, our cCRE-gene linkage analyses recapitulated regulatory architecture at established AD risk loci in microglia. At the *BIN1* locus, a previously validated microglia-specific enhancer containing rs6733839 and rs72838287 was active in iTF-microglia and linked to *BIN1* via DegCre and ABC. Prior CRISPR excision of this enhancer demonstrated that *BIN1* expression is associated with this regulatory region in microglia,[87] underscoring its functional importance. In our dataset, both variants were predicted to alter TF binding motifs, and notably, the rs72838287 allele associated with decreased AD risk was predicted to weaken a ZSCAN4 motif, consistent with prior eQTL and MPRA evidence linking this allele to reduced *BIN1* expression and regulatory activity.[76] Similarly, rs9357347 was linked to *TREM2* and *TREML2* specifically in untreated iTF-microglia, consistent with prior studies associating this variant with increased *TREM2* expression and reduced AD risk. *TREM2* regulates microglial responses to amyloid pathology and has been associated with altered cerebrospinal fluid Aβ and tau biomarkers, including negative

correlations with tau levels in AD.[75] In our analysis, rs9357347 was predicted to create a ZNF343 motif, consistent with increased enhancer activity and elevated *TREM2* expression observed in prior eQTL studies, supporting a regulatory basis for its protective effect. The ability to recover these well-established disease-associated regulatory relationships in iTF microglia demonstrates that this system captures disease-relevant gene regulation and provides a tractable platform for mechanistic dissection of AD risk variants.

In summary, this study establishes KOLF2.1J iTF-microglia as a rapid and scalable human microglial model that captures key transcriptional and regulatory features of both untreated and activated microglial states. By integrating transcriptomic, epigenomic, and three-dimensional chromatin conformation data, we define TRNs that provide mechanistic context for neurodegenerative disease-associated genetic variation. Beyond this, the multi-omic datasets generated here constitute a comprehensive regulatory atlas that can be leveraged to interrogate microglial gene regulation, prioritize functional variants, and guide future perturbation-based studies. Together, these resources enable systematic dissection of microglial regulatory programs and offer a framework for modeling CNS diseases.

Limitations of the study

This study has several limitations. First, analyses were limited to Day 18 of differentiation. Earlier differentiation stages, as explored with the WTC11 iTF line,[24] could provide critical insight into when microglial TRNs first emerge and how closely these early networks resemble those of bona fide brain microglia. Identifying this temporal window is particularly important for the field, as it would define the stage at which perturbations of microglia-enriched genes or cCREs can still be introduced without disrupting the ability of the cells to acquire microglial identity. Such information would directly inform the design of high-throughput functional assays, including MPRAs and CRISPR-based screens, which are challenging to perform at later stages due to the low transduction and transfection efficiency of fully differentiated microglia. Performing these assays at the iPSC stage, when transduction rates are high, and subsequently differentiating the cells into microglia may help circumvent this limitation.[24] These observations underscore the need for a more detailed temporal map of microglial TRN establishment, which will be essential for guiding future screening efforts and enabling precise functional interrogation of microglial regulatory elements.

Second, our 24 h stimulation was chosen to capture sustained inflammatory programs, a time point frequently used in microglial activation studies and aligned with several published datasets.[17,38,39] However, we acknowledge that NF-κB and interferon signaling are highly dynamic, with autoregulatory feedback loops that vary markedly over time. Earlier stimulation windows would likely reveal transient and immediate-early regulatory events that are not captured at 24 h. These temporal dynamics, combined with the known cross-regulation between NF-κB and interferon pathways, should be considered when interpreting the transcriptional and chromatin landscapes of LPS + IFNγ-treated iTF-microglia.

Third, TRN inferences were based on computational predictions, which can introduce biases. Experimental validation, using tools such as MPRAs, CRISPR perturbations, or ChIP-seq, remains critical for refining these networks.

Finally, while molecular profiling was extensive, functional validation of iTF-microglia was limited. Preliminary assays in KOLF2.1J iTF-microglia confirmed phagocytosis of FITC-labeled beads, GPR34 protein expression (homeostatic marker), and CD38 protein upregulation (inflammatory marker) following LPS + IFNγ treatment. However, these functional data were not included and should be further explored in future studies.

RESOURCE AVAILABILITY

Lead contact

Requests for further information and resources should be directed to and will be fulfilled by the lead contact, J. Nicholas Cochran (ncochran@hudsonalpha.org).

Materials availability

This study did not generate unique reagents.

Data and code availability

- RNA-sequencing, ATAC-sequencing, ChIP-sequencing and Hi-C data have been deposited at GEO database under GEO Superseries: GSE299850 and are publicly available.
- The analysis scripts used to generate the images and statistical output in this study are available on GitHub (https://github.com/HudsonAlpha/iTF-Microglia)
- Any additional information required to reanalyze the data reported in this study is available from the lead contact upon request.

ACKNOWLEDGMENTS

The authors are grateful to Dr. Tess Vessels for assisting with data curation. This study was funded by NIH NIA grant 5R00AG068271 awarded to J.N.C., NIH NIA grant 5R01AG085357 awarded to J.N.C. and R.M.M., Alzheimer's Association AARG-24-1308947 awarded to J.N.C., American Parkinson Disease Association 1269685 to B.B.R., NIH NIGMS 5T32GM146611 awarded to A.G.A., and by generous support from the HudsonAlpha Foundation through the Memory and Mobility Program and the Leo Fund.

AUTHOR CONTRIBUTIONS

Conceptualization, I.R.-N., S.C.B., J.N.C., and R.M.M.; data curation, I.R.-N., A.G.A., and J.W.T.; formal analysis, I.R.-N.; investigation, I.R.-N., S.C.B., S.Q.J., B.B.R., A.G.A., S.K.M., and K.M.N.; methodology, I.R.-N., S.C.B., and J.N.C.; supervision, J.N.C. and R.M.M.; writing – original draft, I.R.-N.; writing – review and editing, I.R.-N., S.C.B., B.B.R., J.N.C., and R.M.M.

DECLARATION OF INTERESTS

The authors declare no competing interests.

STAR★METHODS

Detailed methods are provided in the online version of this paper and include the following:

- KEY RESOURCES TABLE
- EXPERIMENTAL MODEL AND STUDY PARTICIPANT DETAILS
  - KOLF2.1J iTF-iPSCs
- METHOD DETAILS
  - KOLF2.1J iTF-iPSC culture
  - KOLF2.1J iTF-Microglia differentiation

- LPS and IFNγ treatment
- Immunocytochemistry
- RNA-seq library preparation
- ATAC-seq library preparation
- H3K27ac ChIP-seq library preparation
- Hi-C library preparation

- QUANTIFICATION AND STATISTICAL ANALYSIS
  - RNA-seq data analysis
  - RNA-seq meta-analysis
  - ATAC- and ChIP-seq processing and peak calling
  - Hi-C processing and loop calling
  - Nomination of transcriptional regulatory networks (TRNs)
  - Association of TRNs with candidate disease-risk variants

SUPPLEMENTAL INFORMATION

Supplemental information can be found online at https://doi.org/10.1016/j.isci.2026.116412.

Received: September 24, 2025
Revised: March 9, 2026
Accepted: May 29, 2026

REFERENCES

1. Gao, C., Jiang, J., Tan, Y., and Chen, S. (2023). Microglia in neurodegenerative diseases: mechanism and potential therapeutic targets. Signal Transduct. Target. Ther. *8*, 359. https://doi.org/10.1038/s41392-023-01588-0.
2. Prinz, M., and Priller, J. (2014). Microglia and brain macrophages in the molecular age: from origin to neuropsychiatric disease. Nat. Rev. Neurosci. *15*, 300–312. https://doi.org/10.1038/nrn3722.
3. Askarova, A., Yaa, R.M., Marzi, S.J., and Nott, A. (2025). Genetic risk for neurodegenerative conditions is linked to disease-specific microglial pathways. PLoS Genet. *21*, e1011407. https://doi.org/10.1371/journal.pgen.1011407.
4. Adams, L., Song, M.K., Yuen, S., Tanaka, Y., and Kim, Y.-S. (2024). A single-nuclei paired multiomic analysis of the human midbrain reveals age- and Parkinson's disease–associated glial changes. Nat. Aging *4*, 364–378. https://doi.org/10.1038/s43587-024-00583-6.
5. Anderson, A.G., Rogers, B.B., Loupe, J.M., Rodriguez-Nunez, I., Roberts, S.C., White, L.M., Brazell, J.N., Bunney, W.E., Bunney, B.G., Watson, S.J., et al. (2023). Single nucleus multiomics identifies ZEB1 and MAFB as candidate regulators of Alzheimer's disease-specific cis-regulatory elements. Cell Genom. *3*, 100263, *0*. https://doi.org/10.1016/j.xgen.2023.100263.
6. Gamache, J., Gingerich, D., Shwab, E.K., Barrera, J., Garrett, M.E., Hume, C., Crawford, G.E., Ashley-Koch, A.E., and Chiba-Falek, O. (2023). Integrative single-nucleus multi-omics analysis prioritizes candidate cis and trans regulatory networks and their target genes in Alzheimer's disease brains. Cell Biosci. *13*, 185. https://doi.org/10.1186/s13578-023-01120-5.
7. Lee, A.J., Kim, C., Park, S., Joo, J., Choi, B., Yang, D., Jun, K., Eom, J., Lee, S.-J., Chung, S.J., et al. (2023). Characterization of altered molecular mechanisms in Parkinson's disease through cell type–resolved multiomics analyses. Sci. Adv. *9*, eabo2467. https://doi.org/10.1126/sciadv.abo2467.
8. Morabito, S., Miyoshi, E., Michael, N., Shahin, S., Martini, A.C., Head, E., Silva, J., Leavy, K., Perez-Rosendahl, M., and Swarup, V. (2021). Single-nucleus chromatin accessibility and transcriptomic characterization of Alzheimer's disease. Nat. Genet. *53*, 1143–1155. https://doi.org/10.1038/s41588-021-00894-z.
9. Prater, K.E., Green, K.J., Mamde, S., Sun, W., Cochoit, A., Smith, C.L., Chiou, K.L., Heath, L., Rose, S.E., Wiley, J., et al. (2023). Human microglia show unique transcriptional changes in Alzheimer's disease. Nat. Aging *3*, 894–907. https://doi.org/10.1038/s43587-023-00424-y.
10. Sun, N., Victor, M.B., Park, Y.P., Xiong, X., Scannail, A.N., Leary, N., Prosper, S., Viswanathan, S., Luna, X., Boix, C.A., et al. (2023). Human microglial state dynamics in Alzheimer's disease progression. Cell *186*, 4386–4403.e29. https://doi.org/10.1016/j.cell.2023.08.037.
11. Shi, Z., Das, S., Morabito, S., Stocksdale, J., Miyoshi, E., Srinivasan, S.S., Emerson, N., Shahin, A., Rahimzadeh, N., Cao, Z., et al. (2025). Single-nucleus multi-omics identifies shared and distinct pathways in Pick's and Alzheimer's disease. Sci. Adv. *11*, eads7973. https://doi.org/10.1126/sciadv.ads7973.
12. Zhao, Z., Liu, A., Citu, C., Enduru, N., Chen, X., Manuel, A., Sinha, T., Gorski, D., Fernandes, B., Yu, M., et al. (2024). Single-nucleus multiomics reveals the disrupted regulatory programs in three brain regions of sporadic early-onset Alzheimer's disease. Sci. Adv. *11*, eadw4917. https://doi.org/10.21203/rs.3.rs-4622123/v1.
13. Xiong, X., James, B.T., Boix, C.A., Park, Y.P., Galani, K., Victor, M.B., Sun, N., Hou, L., Ho, L.-L., Mantero, J., et al. (2023). Epigenomic dissection of Alzheimer's disease pinpoints causal variants and reveals epigenome erosion. Cell *186*, 4422–4437.e21. https://doi.org/10.1016/j.cell.2023.08.040.
14. Gosselin, D., Skola, D., Coufal, N.G., Holtman, I.R., Schlachetzki, J.C.M., Sajti, E., Jaeger, B.N., O'Connor, C., Fitzpatrick, C., Pasillas, M.P., et al. (2017). An environment-dependent transcriptional network specifies human microglia identity. Science *356*, eaal3222. https://doi.org/10.1126/science.aal3222.
15. Drummond, E., and Wisniewski, T. (2017). Alzheimer's Disease: Experimental Models and Reality. Acta Neuropathol. (Berl.) *133*, 155–175. https://doi.org/10.1007/s00401-016-1662-x.
16. Li, Y.E., Preissl, S., Miller, M., Johnson, N.D., Wang, Z., Jiao, H., Zhu, C., Wang, Z., Xie, Y., Poirion, O., et al. (2023). A comparative atlas of single-cell chromatin accessibility in the human brain. Science *382*, eadf7044. https://doi.org/10.1126/science.adf7044.
17. Abud, E.M., Ramirez, R.N., Martinez, E.S., Healy, L.M., Nguyen, C.H.H., Newman, S.A., Yeromin, A.V., Scarfone, V.M., Marsh, S.E., Fimbres, C., et al. (2017). iPSC-derived human microglia-like cells to study neurological diseases. Neuron *94*, 278–293.e9. https://doi.org/10.1016/j.neuron.2017.03.042.
18. Douvaras, P., Sun, B., Wang, M., Kruglikov, I., Lallos, G., Zimmer, M., Terrenoire, C., Zhang, B., Gandy, S., Schadt, E., et al. (2017). Directed Differentiation of Human Pluripotent Stem Cells to Microglia. Stem Cell Rep. *8*, 1516–1524. https://doi.org/10.1016/j.stemcr.2017.04.023.
19. Guttikonda, S.R., Sikkema, L., Tchieu, J., Saurat, N., Walsh, R.M., Harschnitz, O., Ciceri, G., Sneeboer, M., Mazutis, L., Setty, M., et al. (2021). Fully defined human pluripotent stem cell-derived microglia and tri-culture system model C3 production in Alzheimer's disease. Nat. Neurosci. *24*, 343–354. https://doi.org/10.1038/s41593-020-00796-z.
20. Konttinen, H., Cabral-da-Silva, M. e C., Ohtonen, S., Wojciechowski, S., Shakirzyanova, A., Caligola, S., Giugno, R., Ishchenko, Y., Hernández, D., Fazaludeen, M.F., et al. (2019). PSEN1ΔE9, APPswe, and APOE4 Confer Disparate Phenotypes in Human iPSC-Derived Microglia. Stem Cell Rep. *13*, 669–683. https://doi.org/10.1016/j.stemcr.2019.08.004.
21. McQuade, A., Coburn, M., Tu, C.H., Hasselmann, J., Davtyan, H., and Blurton-Jones, M. (2018). Development and validation of a simplified method to generate human microglia from pluripotent stem cells. Mol. Neurodegener. *13*, 67. https://doi.org/10.1186/s13024-018-0297-x.
22. Muffat, J., Li, Y., Yuan, B., Mitalipova, M., Omer, A., Corcoran, S., Bakiasi, G., Tsai, L.-H., Aubourg, P., Ransohoff, R.M., and Jaenisch, R. (2016). Efficient derivation of microglia-like cells from human pluripotent stem cells. Nat. Med. *22*, 1358–1367. https://doi.org/10.1038/nm.4189.
23. Washer, S.J., Perez-Alcantara, M., Chen, Y., Steer, J., James, W.S., Trynka, G., Bassett, A.R., and Cowley, S.A. (2022). Single-cell transcriptomics defines an improved, validated monoculture protocol for

differentiation of human iPSC to microglia. Sci. Rep. *12*, 19454. https://doi.org/10.1038/s41598-022-23477-2.

24. Dräger, N.M., Sattler, S.M., Huang, C.T.-L., Teter, O.M., Leng, K., Hashemi, S.H., Hong, J., Aviles, G., Clelland, C.D., Zhan, L., et al. (2022). A CRISPRi/a platform in human iPSC-derived microglia uncovers regulators of disease states. Nat. Neurosci. *25*, 1149–1162. https://doi.org/10.1038/s41593-022-01131-4.

25. Volpato, V., and Webber, C. (2020). Addressing variability in iPSC-derived models of human disease: guidelines to promote reproducibility. Dis. Model. Mech. *13*, dmm042317. https://doi.org/10.1242/dmm.042317.

26. Pantazis, C.B., Yang, A., Lara, E., McDonough, J.A., Blauwendraat, C., Peng, L., Oguro, H., Kanaujiya, J., Zou, J., Sebesta, D., et al. (2022). A reference human induced pluripotent stem cell line for large-scale collaborative studies. Cell Stem Cell *29*, 1685–1702.e22. https://doi.org/10.1016/j.stem.2022.11.004.

27. Gracia-Diaz, C., Perdomo, J.E., Khan, M.E., Roule, T., Disanza, B.L., Cajka, G.G., Lei, S., Gagne, A.L., Maguire, J.A., Shalem, O., et al. (2024). KOLF2.1J iPSCs carry CNVs associated with neurodevelopmental disorders. Cell Stem Cell *31*, 288–289. https://doi.org/10.1016/j.stem.2024.02.007.

28. Dobner, J., Nguyen, T., Dunkel, A., Prigione, A., Krutmann, J., and Rossi, A. (2024). Mitochondrial DNA integrity and metabolome profile are preserved in the human induced pluripotent stem cell reference line KOLF2.1J. Stem Cell Rep. *19*, 343–350. https://doi.org/10.1016/j.stemcr.2024.01.009.

29. Dou, D., Holzbaur, E.L.F., and Boecker, C.A. (2025). Protocol for live imaging of axonal transport in iPSC-derived iNeurons. STAR Protoc. *6*, 103556. https://doi.org/10.1016/j.xpro.2024.103556.

30. Martinez-Sanchez, M., Skarnes, W., Jain, A., Vemula, S., Sun, L., Rockowitz, S., and Whitman, M.C. (2025). Chromosome 4 Duplication Associated with Strabismus Leads to Gene Expression Changes in iPSC-Derived Cortical Neurons. Genes *16*, 80. https://doi.org/10.3390/genes16010080.

31. Ryan, M., McDonough, J.A., Ward, M.E., Cookson, M.R., Skarnes, W.C., and Merkle, F.T. (2024). Large structural variants in KOLF2.1J are unlikely to compromise neurological disease modeling. Cell Stem Cell *31*, 290–291. https://doi.org/10.1016/j.stem.2024.02.006.

32. Ki Hong, N., and Alban, O. (2022). Quantitative proteome remodeling characterization of two human reference pluripotent stem cell lines during neurogenesis and cardiomyogenesis. Proteomics *22*, e2100246. https://doi.org/10.1002/pmic.202100246.

33. Ramos, D.M., Skarnes, W.C., Singleton, A.B., Cookson, M.R., and Ward, M.E. (2021). Tackling neurodegenerative diseases with genomic engineering: A new stem cell initiative from the NIH. Neuron *109*, 1080–1083. https://doi.org/10.1016/j.neuron.2021.03.022.

34. Fang, K., Pishva, E., Piers, T., and Scholpp, S. (2025). Amyloid-β can activate JNK signalling via WNT5A-ROR2 to reduce synapse formation in Alzheimer's disease. J. Cell Sci. *138*, JCS263526. https://doi.org/10.1242/jcs.263526.

35. Gerrits, E., Heng, Y., Boddeke, E.W.G.M., and Eggen, B.J.L. (2020). Transcriptional profiling of microglia; current state of the art and future perspectives. Glia *68*, 740–755. https://doi.org/10.1002/glia.23767.

36. Mathys, H., Davila-Velderrain, J., Peng, Z., Gao, F., Mohammadi, S., Young, J.Z., Menon, M., He, L., Abdurrob, F., Jiang, X., et al. (2019). Single-cell transcriptomic analysis of Alzheimer's disease. Nature *570*, 332–337. https://doi.org/10.1038/s41586-019-1195-2.

37. Li, Q., Cheng, Z., Zhou, L., Darmanis, S., Neff, N.F., Okamoto, J., Gulati, G., Bennett, M.L., Sun, L.O., Clarke, L.E., et al. (2019). Developmental Heterogeneity of Microglia and Brain Myeloid Cells Revealed by Deep Single-Cell RNA Sequencing. Neuron *101*, 207–223.e10. https://doi.org/10.1016/j.neuron.2018.12.006.

38. Egger, F., Jakab, M., Fuchs, J., Oberascher, K., Brachtl, G., Ritter, M., Kerschbaum, H.H., and Gaisberger, M. (2020). Effect of Glycine on BV-2 Microglial Cells Treated with Interferon-γ and Lipopolysaccharide. Int. J. Mol. Sci. *21*, 804. https://doi.org/10.3390/ijms21030804.

39. Reed, K.S.M., Davis, E.S., Bond, M.L., Cabrera, A., Thulson, E., Quiroga, I.Y., Cassel, S., Woolery, K.T., Hilton, I., Won, H., et al. (2022). Temporal analysis suggests a reciprocal relationship between 3D chromatin structure and transcription. Cell Rep. *41*, 111567. https://doi.org/10.1016/j.celrep.2022.111567.

40. Carter, S.L., Müller, M., Manders, P.M., and Campbell, I.L. (2007). Induction of the genes for Cxcl9 and Cxcl10 is dependent on IFN-gamma but shows differential cellular expression in experimental autoimmune encephalomyelitis and by astrocytes and microglia in vitro. Glia *55*, 1728–1739. https://doi.org/10.1002/glia.20587.

41. Mclellan, H., Heiser, A., and Hart, D.N. (1999). Induction of dendritic cell costimulator molecule expression is suppressed by T cells in the absence of antigen-specific signalling: role of cluster formation, CD40 and HLA-class II for dendritic cell activation. Immunology *98*, 171–180. https://doi.org/10.1046/j.1365-2567.1999.00860.x.

42. Rauf, A., Badoni, H., Abu-Izneid, T., Olatunde, A., Rahman, M., Painuli, S., Semwal, P., Wilairatana, P., and Mubarak, M. (2022). Neuroinflammatory Markers: Key Indicators in the Pathology of Neurodegenerative Diseases. Molecules *27*, 3194. https://doi.org/10.3390/molecules27103194.

43. You, J.-E., Kim, E.-J., Kim, H.W., Kim, J.-S., Kim, K., and Kim, P.-H. (2024). Exploring the Role of Guanylate-Binding Protein-2 in Activated Microglia-Mediated Neuroinflammation and Neuronal Damage. Biomedicines *12*, 1130. https://doi.org/10.3390/biomedicines12051130.

44. (2007). Regulation of Interferon-γ During Innate and Adaptive Immune Responses. In Advances in ImmunologyAdvances in Immunology (Academic Press), pp. 41–101. https://doi.org/10.1016/S0065-2776(07)96002-2.

45. Pallotta, M.T., Rossini, S., Suvieri, C., Coletti, A., Orabona, C., Macchiarulo, A., Volpi, C., and Grohmann, U. (2022). Indoleamine 2,3-dioxygenase 1 (IDO1): an up-to-date overview of an eclectic immunoregulatory enzyme. FEBS J. *289*, 6099–6118. https://doi.org/10.1111/febs.16086.

46. Green, G.S., Fujita, M., Yang, H.-S., Taga, M., Cain, A., McCabe, C., Comandante-Lou, N., White, C.C., Schmidtner, A.K., Zeng, L., et al. (2024). Cellular communities reveal trajectories of brain ageing and Alzheimer's disease. Nature *633*, 634–645. https://doi.org/10.1038/s41586-024-07871-6.

47. Stępniak, K., Machnicka, M.A., Mieczkowski, J., Macioszek, A., Wojtaś, B., Gielniewski, B., Poleszak, K., Perycz, M., Król, S.K., Guzik, R., et al. (2021). Mapping chromatin accessibility and active regulatory elements reveals pathological mechanisms in human gliomas. Nat. Commun. *12*, 3621. https://doi.org/10.1038/s41467-021-23922-2.

48. Moore, J.E., Pratt, H.E., Fan, K., Phalke, N., Fisher, J., Elhajjajy, S.I., Andrews, G., Gao, M., Shedd, N., Fu, Y., et al. (2026). An expanded registry of candidate cis-regulatory elements. Nature, 1–10. https://doi.org/10.1038/s41586-025-09909-9.

49. Dobner, J., Diecke, S., Krutmann, J., Prigione, A., and Rossi, A. (2024). Reassessment of marker genes in human induced pluripotent stem cells for enhanced quality control. Nat. Commun. *15*, 8547. https://doi.org/10.1038/s41467-024-52922-1.

50. Yeh, F.L., Hansen, D.V., and Sheng, M. (2017). TREM2, Microglia, and Neurodegenerative Diseases. Trends Mol. Med. *23*, 512–533. https://doi.org/10.1016/j.molmed.2017.03.008.

51. Rogers, B.B., and Cochran, J.N. (2025). Non-coding variation in dementias: mechanisms, insights, and challenges. NPJ Dement. *1*, 9. https://doi.org/10.1038/s44400-025-00012-4.

52. Field, A., and Adelman, K. (2020). Evaluating Enhancer Function and Transcription. Annu. Rev. Biochem. *89*, 213–234. https://doi.org/10.1146/annurev-biochem-011420-095916.

53. Herrera-Uribe, J., Liu, H., Byrne, K.A., Bond, Z.F., Loving, C.L., and Tuggle, C.K. (2020). Changes in H3K27ac at Gene Regulatory Regions in Porcine Alveolar Macrophages Following LPS or PolyIC Exposure. Front. Genet. *11*, 817. https://doi.org/10.3389/fgene.2020.00817.

54. Huang, M., Malovic, E., Ealy, A., Jin, H., Anantharam, V., Kanthasamy, A., and Kanthasamy, A.G. (2023). Microglial immune regulation by epigenetic reprogramming through histone H3K27 acetylation in neuroinflammation. Front. Immunol. *14*, 1052925. https://doi.org/10.3389/fimmu.2023.1052925.

55. Machlab, D., Burger, L., Soneson, C., Rijli, F.M., Schübeler, D., and Stadler, M.B. (2022). monaLisa: an R/Bioconductor package for identifying regulatory motifs. Bioinformatics *38*, 2624–2625. https://doi.org/10.1093/bioinformatics/btac102.

56. Abdelalim, E.M., Emara, M.M., and Kolatkar, P.R. (2014). The SOX transcription factors as key players in pluripotent stem cells. Stem Cells Dev. *23*, 2687–2699. https://doi.org/10.1089/scd.2014.0297.

57. Yusa, K., Rad, R., Takeda, J., and Bradley, A. (2009). Generation of transgene-free induced pluripotent mouse stem cells by the piggyBac transposon. Nat. Methods *6*, 363–369. https://doi.org/10.1038/nmeth.1323.

58. Huang, P., Zhu, J., Liu, Y., Liu, G., Zhang, R., Li, D., Pei, D., and Zhu, P. (2021). Identification of New Transcription Factors that Can Promote Pluripotent Reprogramming. Stem Cell Rev. Rep. *17*, 2223–2234. https://doi.org/10.1007/s12015-021-10220-z.

59. Chen, S.-W., Hung, Y.-S., Fuh, J.-L., Chen, N.-J., Chu, Y.-S., Chen, S.-C., Fann, M.-J., and Wong, Y.-H. (2021). Efficient conversion of human induced pluripotent stem cells into microglia by defined transcription factors. Stem Cell Rep. *16*, 1363–1380. https://doi.org/10.1016/j.stemcr.2021.03.010.

60. Ballasch, I., García-García, E., Vila, C., Pérez-González, A., Sancho-Balsells, A., Fernández, J., Soto, D., Puigdellívol, M., Gasull, X., Alberch, J., et al. (2023). Ikzf1 as a novel regulator of microglial homeostasis in inflammation and neurodegeneration. Brain Behav. Immun. *109*, 144–161. https://doi.org/10.1016/j.bbi.2023.01.016.

61. Yamasaki, A., Imanishi, I., Tanaka, K., Ohkawa, Y., Tsuda, M., and Masuda, T. (2024). IRF8 and MAFB drive distinct transcriptional machineries in different resident macrophages of the central nervous system. Commun. Biol. *7*, 896. https://doi.org/10.1038/s42003-024-06607-6.

62. Gao, T., Jernigan, J., Raza, S.A., Dammer, E.B., Xiao, H., Seyfried, N.T., Levey, A.I., and Rangaraju, S. (2019). Transcriptional regulation of homeostatic and disease-associated-microglial genes by IRF1, LXRβ and CEBPα. Glia *67*, 1958–1975. https://doi.org/10.1002/glia.23678.

63. Yeh, H., and Ikezu, T. (2019). Transcriptional and epigenetic regulation of microglia in health and disease. Trends Mol. Med. *25*, 96–111. https://doi.org/10.1016/j.molmed.2018.11.004.

64. Zhang, G., Lu, J., Zheng, J., Mei, S., Li, H., Zhang, X., Ping, A., Gao, S., Fang, Y., and Yu, J. (2024). Spi1 regulates the microglial/macrophage inflammatory response via the PI3K/AKT/mTOR signaling pathway after intracerebral hemorrhage. Neural Regen. Res. *19*, 161–170. https://doi.org/10.4103/1673-5374.375343.

65. Papageorgiou, I.E., Lewen, A., Galow, L.V., Cesetti, T., Scheffel, J., Regen, T., Hanisch, U.-K., and Kann, O. (2016). TLR4-activated microglia require IFN-γ to induce severe neuronal dysfunction and death in situ. Proc. Natl. Acad. Sci. USA *113*, 212–217. https://doi.org/10.1073/pnas.1513853113.

66. Wang, L., Zhu, Y., Zhang, N., Xian, Y., Tang, Y., Ye, J., Reza, F., He, G., Wen, X., and Jiang, X. (2024). The multiple roles of interferon regulatory factor family in health and disease. Signal Transduct. Target. Ther. *9*, 282. https://doi.org/10.1038/s41392-024-01980-4.

67. Young, A.P., and Denovan-Wright, E.M. (2024). JAK1/2 Regulates Synergy Between Interferon Gamma and Lipopolysaccharides in Microglia. J. Neuroimmune Pharmacol. *19*, 14. https://doi.org/10.1007/s11481-024-10115-z.

68. Bellenguez, C., Küçükali, F., Jansen, I.E., Kleineidam, L., Moreno-Grau, S., Amin, N., Naj, A.C., Campos-Martin, R., Grenier-Boley, B., Andrade, V., et al. (2022). New insights into the genetic etiology of Alzheimer's disease and related dementias. Nat. Genet. *54*, 412–436. https://doi.org/10.1038/s41588-022-01024-z.

69. Gusev, A., Lee, S.H., Trynka, G., Finucane, H., Vilhjálmsson, B.J., Xu, H., Zang, C., Ripke, S., Bulik-Sullivan, B., Stahl, E., et al. (2014). Partitioning Heritability of Regulatory and Cell-Type-Specific Variants across 11 Common Diseases. Am. J. Hum. Genet. *95*, 535–552. https://doi.org/10.1016/j.ajhg.2014.10.004.

70. Finucane, H.K., Bulik-Sullivan, B., Gusev, A., Trynka, G., Reshef, Y., Loh, P.-R., Anttila, V., Xu, H., Zang, C., Farh, K., et al. (2015). Partitioning heritability by functional annotation using genome-wide association summary statistics. Nat. Genet. *47*, 1228–1235. https://doi.org/10.1038/ng.3404.

71. de Leeuw, C.A., Mooij, J.M., Heskes, T., and Posthuma, D. (2015). MAGMA: Generalized Gene-Set Analysis of GWAS Data. PLoS Comput. Biol. *11*, e1004219. https://doi.org/10.1371/journal.pcbi.1004219.

72. Coetzee, S.G., Coetzee, G.A., and Hazelett, D.J. (2015). motifbreakR: an R/Bioconductor package for predicting variant effects at transcription factor binding sites. Bioinformatics *31*, 3847–3849. https://doi.org/10.1093/bioinformatics/btv470.

73. Anderson, A.G., Moyers, B.A., Loupe, J.M., Rodriguez-Nunez, I., Felker, S.A., Lawlor, J.M.J., Bunney, W.E., Bunney, B.G., Cartagena, P.M., Sequeira, A., et al. (2024). Allele-specific transcription factor binding across human brain regions offers mechanistic insight into eQTLs. Genome Res. *34*, 1224–1234. https://doi.org/10.1101/gr.278601.123.

74. Carrasquillo, M.M., Allen, M., Burgess, J.D., Wang, X., Strickland, S.L., Aryal, S., Siuda, J., Kachadoorian, M.L., Medway, C., Younkin, C.S., et al. (2017). A candidate regulatory variant at the TREM gene cluster associates with decreased Alzheimer's disease risk and increased TREML1 and TREM2 brain gene expression. Alzheimer's Dement. *13*, 663–673. https://doi.org/10.1016/j.jalz.2016.10.005.

75. Tian, M.-L., Ni, X.-N., Li, J.-Q., Tan, C.-C., Cao, X.-P., and Tan, L. (2019). A Candidate Regulatory Variant at the TREM Gene Cluster Confer Alzheimer's Disease Risk by Modulating Both Amyloid-β Pathology and Neuronal Degeneration. Front. Neurosci. *13*, 742. https://doi.org/10.3389/fnins.2019.00742.

76. Bond, M.L., Quiroga-Barber, I.Y., D'Costa, S., Wu, Y., Bell, J.L., McAfee, J.C., Kramer, N.E., Lee, S., Patrucco, M., Phanstiel, D.H., et al. (2024). Deciphering the functional impact of Alzheimer's Disease-associated variants in resting and proinflammatory immune cells. Preprint at medRxiv. https://doi.org/10.1101/2024.09.13.24313654.

77. Platanitis, E., and Decker, T. (2018). Regulatory Networks Involving STATs, IRFs, and NFκB in Inflammation. Front. Immunol. *9*, 2542. https://doi.org/10.3389/fimmu.2018.02542.

78. Qiao, Y., Giannopoulou, E.G., Chan, C.H., Park, S.h., Gong, S., Chen, J., Hu, X., Elemento, O., and Ivashkiv, L.B. (2013). Synergistic Activation of Inflammatory Cytokine Genes by Interferon-γ-Induced Chromatin Remodeling and Toll-like Receptor Signaling. Immunity *39*, 454–469. https://doi.org/10.1016/j.immuni.2013.08.009.

79. Hammond, T.R., Marsh, S.E., and Stevens, B. (2019). Immune Signaling in Neurodegeneration. Immunity *50*, 955–974. https://doi.org/10.1016/j.immuni.2019.03.016.

80. Kann, O., Almouhanna, F., and Chausse, B. (2022). Interferon γ: a master cytokine in microglia-mediated neural network dysfunction and neurodegeneration. Trends Neurosci. *45*, 913–927. https://doi.org/10.1016/j.tins.2022.10.007.

81. Kosoy, R., Fullard, J.F., Zeng, B., Bendl, J., Dong, P., Rahman, S., Kleopoulos, S.P., Shao, Z., Girdhar, K., Humphrey, J., et al. (2022). Genetics of the human microglia regulome refines Alzheimer's disease risk loci. Nat. Genet. *54*, 1145–1154. https://doi.org/10.1038/s41588-022-01149-1.

82. Huang, K.l., Marcora, E., Pimenova, A.A., Di Narzo, A.F., Kapoor, M., Jin, S.C., Harari, O., Bertelsen, S., Fairfax, B.P., Czajkowski, J., et al. (2017). A common haplotype lowers PU.1 expression in myeloid cells and delays onset of Alzheimer's disease. Nat. Neurosci. *20*, 1052–1061. https://doi.org/10.1038/nn.4587.

83. Sun, E., Motolani, A., Campos, L., and Lu, T. (2022). The Pivotal Role of NF-kB in the Pathogenesis and Therapeutics of Alzheimer's Disease. Int. J. Mol. Sci. *23*, 8972. https://doi.org/10.3390/ijms23168972.

84. Yan, Z., Gibson, S.A., Buckley, J.A., Qin, H., and Benveniste, E.N. (2018). Role of the JAK/STAT signaling pathway in regulation of innate immunity in neuroinflammatory diseases. Clin. Immunol. Orlando Fla *189*, 4–13. https://doi.org/10.1016/j.clim.2016.09.014.

85. Hoenen, C., Gustin, A., Birck, C., Kirchmeyer, M., Beaume, N., Felten, P., Grandbarbe, L., Heuschling, P., and Heurtaux, T. (2016). Alpha-Synuclein Proteins Promote Pro-Inflammatory Cascades in Microglia: Stronger Effects of the A53T Mutant. PLoS One *11*, e0162717. https://doi.org/10.1371/journal.pone.0162717.

86. Kozlova, A., Zhang, S., Sudwarts, A., Zhang, H., Smirnou, S., Byeon, S.K., Thapa, C., Sun, X., Stephenson, K., Zhao, X., et al. (2025). PICALM Alzheimer's risk allele causes abberrant lipid droplets in microglia. Nature *646*, 1178–1186. https://doi.org/10.1038/s41586-025-09486-x.

87. Nott, A., Holtman, I.R., Coufal, N.G., Schlachetzki, J.C.M., Yu, M., Hu, R., Han, C.Z., Pena, M., Xiao, J., Wu, Y., et al. (2019). Brain cell type–specific enhancer–promoter interactome maps and disease-risk association. Science *366*, 1134–1139. https://doi.org/10.1126/science.aay0793.

88. Patro, R., Duggal, G., Love, M.I., Irizarry, R.A., and Kingsford, C. (2017). Salmon provides fast and bias-aware quantification of transcript expression. Nat. Methods *14*, 417–419. https://doi.org/10.1038/nmeth.4197.

89. Love, M.I., Huber, W., and Anders, S. (2014). Moderated estimation of fold change and dispersion for RNA-seq data with DESeq2. Genome Biol. *15*, 550. https://doi.org/10.1186/s13059-014-0550-8.

90. Milacic, M., Beavers, D., Conley, P., Gong, C., Gillespie, M., Griss, J., Haw, R., Jassal, B., Matthews, L., May, B., et al. (2024). The Reactome Pathway Knowledgebase 2024. Nucleic Acids Res. *52*, D672–D678. https://doi.org/10.1093/nar/gkad1025.

91. Yu, G., Wang, L.-G., Han, Y., and He, Q.-Y. (2012). clusterProfiler: an R Package for Comparing Biological Themes Among Gene Clusters. OMICS A J. Integr. Biol. *16*, 284–287. https://doi.org/10.1089/omi.2011.0118.

92. The ENCODE Project Consortium (2012). An integrated encyclopedia of DNA elements in the human genome. Nature *489*, 57–74. https://doi.org/10.1038/nature11247.

93. Lun, A.T.L., and Smyth, G.K. (2016). csaw: a Bioconductor package for differential binding analysis of ChIP-seq data using sliding windows. Nucleic Acids Res. *44*, e45. https://doi.org/10.1093/nar/gkv1191.

94. Roberts, B.S., Anderson, A.G., Partridge, E.C., Cooper, G.M., and Myers, R.M. (2024). Probabilistic association of differentially expressed genes with cis-regulatory elements. Genome Res. *34*, 620–632. https://doi.org/10.1101/gr.278598.123.

95. Fulco, C.P., Nasser, J., Jones, T.R., Munson, G., Bergman, D.T., Subramanian, V., Grossman, S.R., Anyoha, R., Doughty, B.R., Patwardhan, T.A., et al. (2019). Activity-by-contact model of enhancer–promoter regulation from thousands of CRISPR perturbations. Nat. Genet. *51*, 1664–1669. https://doi.org/10.1038/s41588-019-0538-0.

96. Love, M.I., Soneson, C., Hickey, P.F., Johnson, L.K., Pierce, N.T., Shepherd, L., Morgan, M., and Patro, R. (2020). Tximeta: Reference sequence checksums for provenance identification in RNA-seq. PLoS Comput. Biol. *16*, e1007664. https://doi.org/10.1371/journal.pcbi.1007664.

97. Buenrostro, J.D., Wu, B., Chang, H.Y., and Greenleaf, W.J. (2015). ATAC-seq: A Method for Assaying Chromatin Accessibility Genome-Wide. Curr. Protoc. Mol. Biol. *109*, 21.29.1–21.29.9. https://doi.org/10.1002/0471142727.mb2129s109.

98. Gu, Z., and Hübschmann, D. (2023). rGREAT: an R/bioconductor package for functional enrichment on genomic regions. Bioinformatics *39*, btac745. https://doi.org/10.1093/bioinformatics/btac745.

99. Liberzon, A., Subramanian, A., Pinchback, R., Thorvaldsdóttir, H., Tamayo, P., and Mesirov, J.P. (2011). Molecular signatures database (MSigDB) 3.0. Bioinformatics *27*, 1739–1740. https://doi.org/10.1093/bioinformatics/btr260.

STAR★METHODS

KEY RESOURCES TABLE

REAGENT or RESOURCE	SOURCE	IDENTIFIER
Antibodies		
Phalloidin Labeling Probes	ThermoFisher	A12379
IBA1 Monoclonal Antibody (GT10312)	ThermoFisher	MA5-27726; RRID: AB_2735228
CD11b Monoclonal Antibody (M1/70), Alexa Fluor™ 488, eBioscience™	ThermoFisher	53-0112-82; RRID: AB_469901
DAPI Nucleic Acid Stain	ThermoFisher	62248
Anti-H3K27ac	ActiveMotif	39034; RRID: AB_2561016
Alexa 488 Goat-AntiMouse	ThermoFisher	A-11001; RRID: AB_2534069
Chemicals, peptides, and recombinant proteins		
Growth Factor Reduced (GFR), LDEV-Free Matrigel	Corning	354230
ReLeSR	StemCell Technologies	100–0483
mTeSR Plus medium	StemCell Technologies	100–0276
Essential 8 Basal Medium	ThermoFisher	A1517001
Y-27632 (ROCK) Inhibitor	StemCell Technologies	72304
Doxycycline	StemCell Technologies	72742
Lipopolysaccharide (LPS)	Invitrogen	50-112-2025
Interferon-gamma (IFNy)	ThermoFisher	PHC4031
Advanced DMEM/F12	ThermoFisher	12634010
GlutaMAX	ThermoFisher	35050061
Human IL-34	PeproTech	200-34-50UG
Human GM-CSF	PeproTech	300-03-5UG
M-CSF	PeproTech	300-25-50UG
Human TGF-B1	PeproTech	100-21-10UG
TritonX	Sigma	X100-100ML
ProLong Diamond Antifade mountant	ThermoFisher	P36961
Lipopolysaccharide (LPS)	Invitrogen	50-112-2025
Interferon-gamma (IFNy)	ThermoFisher	PHC4031
Critical commercial assays		
Total RNA Purification Plus Kit	Norgen	17270
Tagment DNA TDE1 Enzyme and Buffer	Illumina	20034197
Q5 HotStart Master Mix	NEB	M0494S
Arima-HiC+ Genome-Wide Hi-C Kit	Arima Genomics	A410232
Deposited data		
Raw and analyzed data- Accession code GEO: GSE299850	This study	https://www.ncbi.nlm.nih.gov/geo/query/acc.cgi?acc=GSE299850
Experimental models: Cell lines		
KOLF2.1J CLYBL_6-TF-iMG_KI1/KI2 iPSCs	The Jackson Laboratory	JIPSC002072
Oligonucleotides		
Nextera XT Index Primers	Illumina	FC-131-1001
Software and algorithms		
Salmon	Patro et al.[88]	https://combine-lab.github.io/salmon/
DESeq2	Love et al.[89]	https://bioconductor.org/packages/release/bioc/html/DESeq2.html
Reactome	Milacic et al.[90]	https://reactome.org/

(*Continued on next page*)

Continued

REAGENT or RESOURCE	SOURCE	IDENTIFIER
clusterProfiler	Yu et al.[91]	https://bioconductor.org/packages/release/bioc/html/clusterProfiler.html
ENCODE ATAC-seq pipeline v1.7.0	ENCODE Consortium[92]	https://github.com/ENCODE-DCC/atac-seq-pipeline
csaw	Lun and Smyth[93]	https://bioconductor.org/packages/release/bioc/html/csaw.html
DegCre	Roberts et al.[94]	https://bioconductor.org/packages//release/bioc/html/DegCre.html
Activity by Contact	Fulco et al.[95]	https://github.com/broadinstitute/ABC-Enhancer-Gene-Prediction
monaLisa	Machlab et al.[55]	https://bioconductor.org/packages/release/bioc/html/monaLisa.html
sLDSC v1.0.1	Finucane et al.[70]	https://github.com/bulik/ldsc
MAGMA v1.10	De Leeuw et al.[71]	https://github.com/neurogenomics/MAGMA_Celltyping
motifbreakR	Coetzee et al.[72]	https://bioconductor.org/packages/release/bioc/html/motifbreakR.html
tximeta	Love et al.[96]	https://bioconductor.org/packages/release/bioc/html/tximeta.html
R v4.3	CRAN	https://cran.r-project.org
Code	This study	https://github.com/HudsonAlpha/iTF-Microglia

EXPERIMENTAL MODEL AND STUDY PARTICIPANT DETAILS

KOLF2.1J iTF-iPSCs

KOLF2.1J CLYBL_6-TF-iMG_KI1/KI2 iPSCs (JIPSC002072), hereafter referred to as iTF-iPSCs, were obtained from The Jackson Laboratory. Notably, the KOLF2.1J iTF-iPSC line used in this study contains a single genomic insertion site (CLBYL safer harbor locus) encoding all six TFs, in contrast to the dual insertion sites used by Dräger et al.,[24] in which three TFs were inserted at the AAVS1 safe harbor locus and three at the CLBYL locus. iTF-iPSCs were authenticated and pathogen tested by The Jackson Laboratory.

METHOD DETAILS

KOLF2.1J iTF-iPSC culture

Cells were maintained at 37°C with 5% CO_2 in mTeSR Plus medium (StemCell Technologies) on dishes coated with Growth Factor Reduced (GFR), LDEV-Free Matrigel (Corning). Medium was changed every other day. Cells were passaged at 70–80% confluency using ReLeSR (StemCell Technologies), resuspended in room temperature mTeSR Plus, and transferred to freshly coated dishes.

KOLF2.1J iTF-Microglia differentiation

Differentiation was performed following the Dräger et al. protocol[24] with minor modifications. iTF-iPSCs were washed with D-PBS, dissociated with Accutase (StemCell Technologies), and centrifuged at 300×g for 5 min. Cell pellets were resuspended in Essential 8 Basal Medium (ThermoFisher) supplemented with 10 μM Y-27632 (ROCK) Inhibitor and 2 μg/mL doxycycline (StemCell Technologies), then seeded onto double-coated plates with Poly-D-Lysine-precoated Bio plates (Corning) and GFR Matrigel.

On day 2, cells were switched to differentiation medium (Advanced DMEM/F12 (Gibco) supplemented with 1× GlutaMAX (Gibco), 2 μg/mL doxycycline, 100 ng/mL human IL-34 and 10 ng/mL human GM-CSF (PeproTech)). On day 4, the medium was replaced with iTF-Microglia medium (Advanced DMEM/F12 supplemented with 1× GlutaMAX, 2 μg/mL doxycycline, 100 ng/mL human IL-34, 10 ng/mL human GM-CSF, 50 ng/mL human M-CSF and 50 ng/mL human TGF-β1 (PeproTech). On day 8, media was renewed with fresh iTF-Microglia medium. Cells were maintained for 9 more days with full medium changes every 2–3 days.

LPS and IFNγ treatment

iTF-iPSCs and iTF-Microglia on day 17 of differentiation were either untreated or stimulated with 100 ng/mL Lipopolysaccharide (LPS; Invitrogen) and 20 ng/mL interferon-gamma (IFNγ;Gibco) in fresh mTeSR Plus (for iTF-iPSCs) or iTF-Microglia medium (for

iTF-Microglia) for 24 h before harvesting. A 24 h stimulation period was selected to induce a robust inflammatory response and to capture both the primary transcriptional changes and downstream regulatory programs associated with a sustained inflammatory state, as demonstrated in previous studies.[17,38,39]

Immunocytochemistry

Immunocytochemistry was performed on iTF-Microglia differentiated for two weeks that were either untreated or treated with LPS + IFNγ for 24 h (see above). Cells were first fixed for 10 min at room temperature in a 4% formaldehyde solution (ThermoFisher #PI28908) in ultra-pure water. After fixation, cells were dried for 5 min and washed four times with PBS (Corning #21-040-CV). Cells were then permeabilized and blocked for 1 h in 5% BSA in PBS with 0.1% TritonX at 4°C. Cells were then incubated overnight in primary antibodies diluted in 5% BSA in PBS at 4°C. The next day, cells were washed four times with PBS then, if primary was unconjugated, incubated with fluorescently conjugated secondary antibodies and DAPI (Thermo #62248) in 5% BSA in PBS for 1 h at room temperature. Stained cells were then washed four times with PBS and mounted with ProLong Diamond Antifade mountant (ThermoFisher #P36961) and imaged on a BioTek LionHeart FX automated live cell imager with BioTek Gen5 (v3.4) control and data analysis software. All cells were stained with either 0.25*X* Phalloidin (Thermo #A12379), 0.25 μg/mL IBA1 (Thermo #MA5-27726), or 0.5 μg/mL CD11B (Thermo #53-0112-82). Cells stained with IBA1 were also stained with Alexa 488 Goat-AntiMouse (Thermo #A-11001) at a 1:1,000 dilution.

RNA-seq library preparation

RNA-seq was performed in triplicate per condition, with a replicate defined as an independent grow up and differentiation (for iTF-microglia). Total RNA was extracted from untreated and LPS + IFNγ-treated iTF-iPSCs and iTF-Microglia using the Total RNA Purification Plus Kit (Norgen). RNA concentration was measured with the Qubit RNA HS Assay Kit (ThermoFisher). Library preparation and paired-end 150 bp (PE150) sequencing were performed by Novogene on an Illumina NovaSeq X Plus platform.

ATAC-seq library preparation

ATAC-seq was performed in duplicate, with a replicate defined as an independent grow up and differentiation (for iTF-microglia). ATAC-seq was performed on untreated iTF-iPSCs, and untreated and LPS + IFNγ-treated iTF-Microglia following a published protocol.[97] Briefly, 100,000 cells were harvested by mechanical dissociation, washed with 50 μL cold 1*X* PBS, and centrifuged at 300×g for 5 min. The pellet was resuspended in 50 μL cold lysis buffer (10 mM Tris-HCl pH 7.5, 10 mM NaCl, 3 mM $MgCl_2$, 0.1% NP-40, 0.1% Tween 20, 0.01% Digitonin, and nuclease-free H_2O) and incubated for 3 min on ice. After lysis, 1 mL of wash buffer (10 mM Tris-HCl pH 7.5, 10 mM NaCl, 3 mM $MgCl_2$, 0.1% Tween 20, and nuclease-free H_2O) was added, mixed by gentle inversion, and centrifuged at 500×g for 10 min at 4°C. The nuclei pellet was resuspended in 50 μL transposition mix (Tagment DNA TDE1 Enzyme and Buffer, Illumina) and incubated at 37°C for 30 min with shaking (1000 rpm). DNA was purified using the Qiagen MinElute Reaction Cleanup Kit and eluted in 11 μL.

Libraries were generated using Nextera XT Index primers (Illumina) and Q5 Hot Start Master Mix (NEB), followed by PCR amplification (30 s at 98°C; [10 s at 98°C, 30 s at 63°C, 1 min at 72°C] ×10 cycles). Libraries were quantified using the Qubit dsDNA HS Assay Kit and quality-checked with an Agilent BioAnalyzer High Sensitivity DNA chip. Sequencing was performed on an Illumina NovaSeq X Plus (PE150), targeting ∼200 million reads per library.

H3K27ac ChIP-seq library preparation

ChIP-seq for H3K27ac was performed in duplicate, with a replicate defined as an independent grow up and differentiation (for iTF-microglia) on chromatin from untreated iTF-iPSCs, and untreated and LPS + IFNγ-treated iTF-Microglia, following protocols from the ENCODE Consortium.[92] Briefly, chromatin was immunoprecipitated with an anti-H3K27ac antibody (ActiveMotif). Libraries were prepared by end-repair, adapter ligation, and PCR amplification (30 s at 98°C; [10 s at 98°C, 30 s at 65°C, 30 s at 72°C] ×15 cycles; 5 min at 72°C). Libraries were quantified with the Qubit dsDNA HS Assay Kit and analyzed with the Standard Sensitivity NGS Fragment Analysis Kit (Advanced Analytical) on an Agilent Fragment Analyzer 5200. Sequencing was performed on an Illumina NovaSeq X Plus (PE150), targeting ∼30 million reads per library.

Hi-C library preparation

Hi-C libraries were generated in duplicate per condition with a replicate defined as an independent grow up and differentiation (for iTF-microglia) using the Arima-HiC+ Genome-Wide Hi-C kit (Arima Genomics) following the manufacturer's protocol. Chromatin from untreated iTF-iPSCs, untreated iTF-Microglia, and LPS + IFNγ-treated iTF-Microglia was crosslinked, digested with restriction enzymes, and proximity-ligated to capture 3D chromatin interactions. Ligated DNA was purified, fragmented, and prepared for sequencing. A pooled 6-plex library was sequenced on an Illumina NovaSeq X Plus 25B lane (PE150), generating 3.3 billion paired-end reads (∼550 million reads per library).

QUANTIFICATION AND STATISTICAL ANALYSIS

All statistical details are provided in the corresponding figure legends. Where statistical significance is indicated by asterisks: $^{*}p < 0.05$, $^{**}p < 0.01$, $^{***}p < 0.001$, and $p < 0.0001$.

RNA-seq data analysis

Raw reads were quality-checked with FastQC before and after trimming. Trim Galore [paired-end mode, –illumina flag] was used to remove adapter sequences and low-quality bases. Trimmed reads were quantified using Salmon [–validateMappings, –seqBias, –gcBias].[88] Reads were mapped to the GENCODE v46 human transcriptome (hg38) using a k-mer size of 31.

Transcript-level quantifications were imported into R with tximeta,[96] and summarized to gene-level using summarizeToGene(). Differential expression analysis was performed with DESeq2[89] after pre-filtering genes with <10 counts in at least three samples. Differentially expressed genes (DEGs) were identified using the Wald test, with contrasts defined between iTF-iPSCs and iTF-Microglia in untreated and LPS + IFNγ-stimulated conditions. Functional enrichment analysis was conducted with clusterProfiler[91] using Reactome pathway annotations.[90]

RNA-seq meta-analysis

Public RNA-seq datasets were obtained from the Gene Expression Omnibus (GEO) to analyze gene expression in iPSCs, iPSC-derived microglia, primary human microglia (n = 6 males and n = 4 females), and blood monocytes. Raw data from Abud et al. (GEO: GSE89189)[17] and Dräger et al. (GEO: GSE178317)[24] were downloaded using the SRA Toolkit (v3.0.0) and converted to FASTQ with fasterq-dump, followed by gzip compression.

FASTQ files from Abud et al. were processed using the same pipeline as above. The Dräger et al. dataset, generated with the QuantSeq 3′ mRNA-Seq Library Prep Kit for Illumina (FWD) (Lexogen), was processed with a custom pipeline. Reads were trimmed with BBDuk to remove adapters and poly-A tail, quality checked with FastQC, and quantified using Salmon [–validateMappings, –noLengthCorrection] and mapped to the GENCODE v46 human transcriptome (hg38) with a k-mer size of 27.

Gene-level counts were analyzed using DESeq2, applying size factor normalization to adjust for library size. Genes with ≥1 normalized count in ≥3 samples were retained. Variance-stabilizing transformation (VST) was applied to stabilize variance across expression levels. Marker genes for iPSCs,[24] microglia and blood monocytes[17] were used to assess cellular identity via hierarchical clustering.

To assess the transcriptional signatures of KOLF2.1J iTF cells in the context of brain cell types and microglial states, we used snRNAseq datasets from postmortem AD and control brains.[46] Marker gene sets from the supplemental tables were formatted as GMT files for gene set enrichment analysis (GSEA) using fgsea.

ATAC- and ChIP-seq processing and peak calling

ATAC-seq data were processed with the ENCODE ATAC-seq pipeline (v1.7.0). Reads were trimmed with Cutadapt, aligned to the hg38 reference genome using Bowtie2, and filtered to remove duplicates and mitochondrial reads using Picard and Samtools. High-quality, properly paired reads were retained. Peaks were called with MACS2 [–shift −75 –extsize 150], filtered for ENCODE blacklist regions, and reproducible peaks identified using IDR and naive overlap. QC measurements and results of the reproducibility test provided by ENCODE are listed in Table S1.

ChIP-seq reads were pre-processed with clumpify (BBMap v38.42) to remove optical duplicates [dedupe = t optical = t dupedist = 12000] and processed with the ENCODE chip-seq-pipeline2 with histone-specific settings [-type histone]. Reads were trimmed with Trimmomatic, aligned to the hg38 reference genome using Bowtie2, and PCR duplicates removed with Picard. Peaks were called with MACS2, and reproducible peaks identified via naive overlap. QC measurements and results of the reproducibility test provided by ENCODE are listed in Table S2.

Hi-C processing and loop calling

Hi-C data were processed using the ENCODE Hi-C pipeline (v1.15.1) following ENCODE standards. Sequencing reads were aligned to the hg38 genome using BWA-MEM. Low-quality, secondary, and duplicate reads were removed, and valid interaction pairs were retained to construct contact matrices at multiple resolutions. A combined.hic file was generated by merging all samples across cell types (iTF-iPSCs and iTF-Microglia) and conditions (untreated and LPS + IFNγ-treated).

Chromatin loops were identified using HiCCUPS, as implemented in the ENCODE Hi-C pipeline. Loops were called from the combined.hic file. Final loop coordinates were extracted from the 30.bedpe.gz output file. QC stats are listed in Table S3.

Nomination of transcriptional regulatory networks (TRNs)

Identification of candidate cis-regulatory elements (cCREs)

cCREs were nominated by overlapping chromatin accessibility (ATAC-seq) and enhancer-associated histone modifications (H3K27ac ChIP-seq). Optimal reproducible peaks from two replicates per dataset were filtered (q-value ≥2) and overlapped using

findOverlaps from the GenomicRanges package. To standardize genomic coordinates across cell types and states, we generated a consensus cCRE set by merging cCREs identified in each condition. Cell-type specific cCREs were then mapped to this consensus set, retaining the consensus coordinates.

Functional enrichment of cCREs was performed using rGREAT[98] with the C2:CP:Reactome pathway collection from the Human Molecular Signatures Database (MSigDB).[99]

Differential accessibility and H3K27ac marking were assessed using the csaw package.[93] ATAC-seq and ChIP-seq reads were quantified within cCREs using regionCounts, normalized using trimmed mean of M-values (TMM) with background bins generated by counting reads in 10 kb non-overlapping windows (windowCounts) across the genome. Differential testing was performed using the edgeR package via csaw. Dispersion estimates were obtained using empirical Bayes shrinkage, and hypothesis testing was conducted using quasi-likelihood F-tests, which provide robust control of false positives in the presence of biological variability between replicates. *p* values were adjusted for multiple testing using the Benjamini-Hochberg method. All identified cCREs are listed in Table S4.

Identification of target genes

We used four complementary approaches to assign target genes to cCREs and TFs: (1) Closest Gene Assignment: Each cCRE was assigned to its nearest gene TSS (GENCODE v46, hg38) using nearest() and distanceToNearest(), restricted to genes with RNA-seq expression >1 TPM. (2) DegCre Analysis: Using DegCre,[94] we correlated DEGs (from DESeq2) with cCREs showing differential accessibility during microglia differentiation (iTF-Microglia vs. iTF-iPSCs) and H3K27ac changes after stimulation (iTF-Microglia-treated LPS + IFNγ vs. iTF-Microglia), from csaw analysis. Only associations with concordant LFC direction and assocAlpha $\leq$0.05 were retained. (3) ABC Model: We applied the ABC model[95] to predict enhancer-gene links based on enhancer activity (ATAC and H3K27ac datasets) and Hi-C contact frequencies (combined.hic file). Predicted enhancer-gene associations were filtered according to published ABC score thresholds,[95] retaining only promoters with scores $\geq$0.1 and enhancers with scores $\geq$0.015. (4) Brain microglia links: We leveraged snMultiomics data from postmortem brains of individuals with and without AD.[5] cCRE-to-gene links were inferred by correlating chromatin accessibility and gene expression within the same nucleus. To maintain relevance to our system, we retained only links involving brain microglia and overlapping our iTF-derived cCREs. Functional enrichment analysis of identified target genes was conducted with clusterProfiler[91] using Reactome pathway annotations.[90]

Identification of TFs in TRNs

To predict TFs driving differential chromatin accessibility during microglial differentiation (iTF-iPSCs vs. iTF-Microglia) and H3K27ac changes upon inflammatory stimulation (LPS + IFNγ-treated iTF-Microglia vs. iTF-Microglia), we applied the monaLisa package.[55] Specifically, we used the randomized lasso stability selection approach to identify TF motifs enriched in cCREs showing changes in accessibility or H3K27ac levels, based on results from csaw. Motif scanning was performed using JASPAR2024 position weight matrices (PWMs) via findMotifHits, with GC content and observed/expected CpG ratios included as covariates to account for sequence bias. TFs were considered significant if their selection probability was $\geq$ 0.8.

Association of TRNs with candidate disease-risk variants

To link TRNs with disease-risk variants, we performed sLDSC (v.1.0.1) analysis with the full baseline-LD v2.2 model[69,70] to test for enrichment of GWAS variants in ATAC and H3K27ac peaks, cCREs and TF-defined cCRE subsets (from monaLisa). For MAGMA (v1.10) analysis,[71] GWAS variants were mapped to gene bodies with a 2 kb upstream window from the TSS. To account for expression-level effects, we performed conditional gene expression analysis using log2(TPM+1) values, filtered for TPM >1, winsorized at 50 TPM, and included as covariates. GWAS summary statistics used for MAGMA and sLDSC analyses are listed in Table S5. For AD GWAS summary statistics, the *APOE* and *HLA* regions were excluded.

To investigate the relevance to neurodegenerative disorders, we intersected TRNs with genetic variants linked to AD (Bellenguez et al.), which we intersected with cCREs from iTF-iPSCs, untreated iTF-Microglia, and LPS + IFNγ-treated iTF-Microglia. To identify TFs whose binding may be disrupted by variants, we used motifbreakR and JASPAR motifs. TF motif disruption was predicted using the "ic" algorithm and PWMs from motifbreakR, with a *p*-value cutoff of $<1 \times 10^{-4}$. Target genes were assigned to candidate variants using DegCre and ABC predictions.